Astronomy & Astrophysics

Chemical abundances in 43 metal-poor stars[★,★★]

K. Jonsell[1], B. Edvardsson[1], B. Gustafsson[1], P. Magain[2], P. E. Nissen[3], and M. Asplund[4]

[1] Department of Astronomy and Space Physics, Uppsala Astronomical Observatory, Box 515, 751 20 Uppsala, Sweden
e-mail: [karin.jonsell;Bengt.Edvardsson;Bengt.Gustafsson]@astro.uu.se
[2] Institut d'Astrophysique et de Géophysique, Université de Liège, Allée du 6 Août 17, 4000 Liège, Belgium
e-mail: Pierre.Magain@ulg.ac.be
[3] Institute of Physics and Astronomy, University of Aarhus, 8000 Aarhus C, Denmark
e-mail: pen@phys.au.dk
[4] Research School of Astronomy and Astrophysics, Mount Stromlo Observatory, Cotter Road, Weston, ACT 2611, Australia
e-mail: martin@mso.anu.edu.au

Abstract. We have derived abundances of O, Na, Mg, Al, Si, Ca, Sc, Ti, V, Cr, Fe, Ni, and Ba for 43 metal-poor field stars in the solar neighbourhood, most of them subgiants or turn-off-point stars with iron abundances [Fe/H] ranging from −0.4 to −3.0. About half of this sample has not been spectroscopically analysed in detail before. Effective temperatures were estimated from *uvby* photometry, and surface gravities primarily from Hipparcos parallaxes. The analysis is differential relative to the Sun, and was carried out with plane-parallel MARCS models. Various sources of error are discussed and found to contribute a total error of about 0.1–0.2 dex for most elements, while relative abundances, such as [Ca/Fe], are most probably more accurate. For the oxygen abundances, determined in an NLTE analysis of the 7774 Å triplet lines, the errors may be somewhat larger. We made a detailed comparison with similar studies and traced the reasons for the, in most cases, relatively small differences.

Among the results we find that [O/Fe] possibly increases beyond [Fe/H] = −1.0, though considerably less so than in results obtained by others from abundances based on OH lines. We did not trace any tendency toward strong overionization of iron, and find the excesses, relative to Fe and the Sun, of the α elements Mg, Si, and Ca to be smaller than those of O. We discuss some indications that also the abundances of different α elements relative to Fe vary and the possibility that some of the scatter around the trends in abundances relative to iron may be real. This may support the idea that the formation of Halo stars occurred in smaller systems with different star formation rates. We verify the finding by Gratton et al. (2003b, A&A, 406, 131) that stars that do not participate in the rotation of the galactic disk show a lower mean and larger spread in [α/Fe] than stars participating in the general rotation. The latter stars also seem to show some correlation between [α/Fe] and rotation speed. We trace some stars with peculiar abundances, among these two Ba stars, HD 17072 and HD 196944, the second already known to be rich in *s* elements. Finally we advocate that a spectroscopic study of a larger sample of halo stars with well-defined selection criteria is very important, in order to add to the very considerable efforts that various groups have already made.

Key words. stars: Population II – stars: fundamental parameters – stars: abundances – Galaxy: halo – Galaxy: abundances – Galaxy: evolution

1. Introduction

One important method of studying the formation and early evolution of galaxies is to explore the properties of the remains of these early events in the Milky Way system. Since the pioneering work by Eggen et al. (1962), investigations of stellar abundances and stellar dynamics have been combined in a large number of studies in attempts to reconstruct the

---

★ Based on observations carried out at the European Southern Observatory, La Silla, Chile.
★★ Tables 1 and 3 are only available in electronic form at the CDS via anonymous ftp to cdsarc.u-strasbg.fr (130.79.128.5) or via http://cdsweb.u-strasbg.fr/cgi-bin/qcat?J/A+A/440/321 Tables 2 and 4 can also be found there.

formation history of the stellar populations. While the homogeneous collapse scenario of Eggen et al. predicted metallicity and age gradients related to the kinematics, the globular clusters were found to show a considerable spread in metal abundances, independent of their distance from the Galactic centre (Searle & Zinn 1978). This instead suggested a scenario of galaxy formation where individual protogalactic systems evolved independently before merging into a larger system. There are a number of indications that the infall and accretion of material after the first collapse phase has played an important role in our Galaxy: the existence of high-latitude and high-velocity interstellar clouds, the relatively small proportion of metal-poor solar-type stars ("the G-dwarf problem"), the large scatter in the age-metallicity relation (if this relation exists at

all) for the Galactic disk, and the discovery of the presently merging Sagittarius dwarf.

More recently, important clues have come from abundance differences in various stellar populations. Thus, Gratton et al. (1996, 2000) and Fuhrmann (1998) have traced significant [α/Fe] ratio (i.e., e.g. Mg, Si, and Ca vs. Fe) differences between the Thick and Thin Galactic disks, suggesting an age difference between the two systems and a period of little or no star-formation in between, possibly marking large-scale in-fall events. Different kinematic properties at a given [Fe/H] may be traced in the disk (see also Bensby et al. 2003). Also two different populations have been traced for the halo stars, as reflected in kinematic properties and [α/Fe] ratios (Nissen & Schuster 1997; Gratton et al. 2003a,b). Gratton et al. distinguish between one population with positive velocity in orbits around the galactic centre and with close correlations between rotational velocity, metallicity, and [α/Fe], and a sec-ond population with small or retrograde orbital velocity with larger scatter in the abundances. The star-to-star scatter in rela-tive abundances, such as in [α/Fe] at a given [Fe/H] for halo stars, may also be used to obtain information on the super-novae, star-formation processes and gas dynamics in the early Galaxy, since supernovae with different initial masses produce different relative amounts of the heavy elements (see Nissen et al. 1994; Karlsson & Gustafsson 2001; Carretta et al. 2002; Arnone et al. 2004; Cayrel et al. 2004).

In order to study the star-to-star scatter, as well as the possible existence of fine structure in the halo-population and the transition to the thick disk population in terms of abun-dances and kinematics, the present project was initiated with observations more than a decade ago. About half of our pro-gramme stars have been independently studied more recently. Our results give checks or support of results obtained by others and add some significant knowledge for understanding Halo formation.

2. Observations and data reductions

43 stars were chosen, mainly from the Olsen (1983) catalogue of Strömgren $uvby - \beta$ photometry and the Olsen (1993) cata-logue of G-dwarfs. The parameters for the stars lie within the following intervals: $4\overset{\mathrm{m}}{.}2 \leq V \leq 9\overset{\mathrm{m}}{.}1$, $0\overset{\mathrm{m}}{.}30 \leq (b - y) \leq 0\overset{\mathrm{m}}{.}51$, and [Me/H] < –0.4. The stars all have $-73° \leq \delta \leq +21°$.

The observations were performed in 1987 and 1988 at the ESO 1.4 m Coudé Auxiliary Telescope, CAT, with the short camera of the Coudé Echelle Spectrometer, CES, equipped with the RCA CCD No. 9. The setup made it possible to ob-tain a spectral resolving power of 60 000 and a signal to noise ratio over about 200. To get a reasonably large sample of un-blended lines of important elements four different wavelength regions were observed: 5670–5720, 6120–6185, 7750–7820, and 8710–8780 Å.

The CCD used in the programme, RCA No. 9, was not fully linear at the time of observation, as found by one of us in a care-ful analysis including simulations of the effects on measured
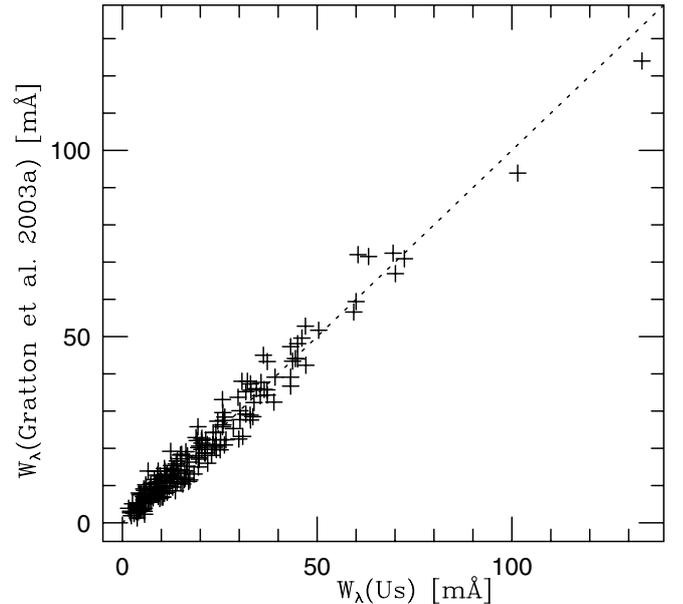
Fig. 1. Comparison of equivalent width measurements with those of Gratton et al. (2003a). The dotted line indicates the 1-to-1 relation.

equivalent widths (Gosset & Magain 1993). To correct for this nonlinearity our equivalent widths, W, were reduced:

$$W_{\mathrm{corrected}} = 0.96 \cdot W_{\mathrm{measured}}. \tag{1}$$

Strong interference fringes appeared in the infrared region. Dome and hot-star flat-fields were used to correct for these.

Up to 62 usable absorption lines were measured. For in-frared lines with equivalent widths under 40 mÅ, the widths were measured with a Gaussian fit. Lines stronger than this were fitted with a Voigt profile. Lines in the visual region of the stellar spectra were measured by a weighted mean between a Gaussian fit and a pure numerical integration. The weight-ing was estimated by eye with respect to suspected blends, line strength, etc. The widths for HD 140283 and HD 196944 in the 7780 Å region are the averages for two spectra. In Fig. 1 we compare our equivalent widths for 212 lines with mea-surements by Gratton et al. (2003a). The mean difference (Us-Gratton et al.) is +0.1 mÅ with a standard deviation of 3.2 mÅ. The adopted equivalent widths are given in Table 1 which is only electronically available.

3. Analysis

3.1. Model atmospheres

3.1.1. Properties of the models

A version of the Uppsala model atmosphere code MARCS was used to calculate the atmospheres for the programme stars, see Asplund et al. (1997).

3.1.2. Fundamental parameters of the atmospheres

The basic stellar data are presented in Table 2.

Effective temperatures. T_{eff} values for the programme stars were derived from Strömgren $uvby - \beta$ photometry collected

Table 2. Data for the 43 stars in the project. Column 1: stellar identification. Column 2: visual apparent magnitude. Column 3: colour index $(b − y)$. Column 4: balmer discontinuity index c_1. Column 5: references for the photometry: 1) Olsen (1983), 2) Schuster & Nissen (1988), 3) Lindgren H. (unpublished), 4) Olsen (1993), 5) Hauck & Mermilliod (1998), 6) Grønbech & Olsen (1976, 1977), 7) SIMBAD. Columns 6–8: stellar space velocities relative to the LSR, see Sect. 3.2. Column 9: stellar masses in units of the Solar mass, see Sect. 3.1.2. Column 10: the effective temperatures. except for HD 196944. Column 11: the metallicities determined from spectroscopy, see Sect. 3.1.2. Column 12: gravitational parameters from Hipparcos parallaxes and evolutionary tracks (VandenBerg et al. 2000), except for HD 196944. Column 13: the classification of the stars according to the SIMBAD database. Column 14: Ba = barium star, b = binary (Nordström et al. 2004), b? = possible binary (Nissen et al. 1997), v = variable (Cayrel de Strobel et al. 1997).

| HD	V mag	$(b − y)$ mag	c_1 mag	Ref.	U km s^{-1}	V km s^{-1}	W km s^{-1}	Mass $M_\odot$	T_{eff} K	[Fe/H] dex	$\log g$	Classification	Notes
17072	6.594	0.441	0.453	1, 2	5	−66	−16	0.80[1]	5428	−0.98	2.65	G2wF5	Ba
25704	8.124	0.371	0.274	1, 2	−119	−62	−1	0.75	5758	−0.97	4.16	F7V	
49301	8.112	0.371	0.408	1	27	−47	21	0.80[1]	5832	−0.82	3.11	F5V	
59374	8.478	0.363	0.273	2	−49	−120	0	0.74	5811	−0.93	4.36	F8V	
61902	8.232	0.327	0.357	1, 2, 3	77	−16	−38	0.99	6105	−0.71	4.04	F5/6wF2	v
63598	7.947	0.358	0.267	2	27	−103	10	0.86	5845	−0.84	4.24	G2V	b
76932	5.806	0.355	0.294	1, 2, 3	−38	−85	77	0.87	5875	−0.89	4.13	F7/F8IV/V	b
78747	7.717	0.385	0.284	1, 3	20	7	−19	0.76	5684	−0.80	4.22	G0/G1V	
79601	8.016	0.382	0.304	4	−10	−35	−29	0.80	5716	−0.74	4.12	G2V	
80863	8.685	0.365	0.304	4	−37	−68	−22	0.80	5834	−0.61	4.26	F7/F8V	b
84937	8.335	0.301	0.359	1, 2, 3	235	−234	0	0.75	6310	−1.96	4.04	sdF5	
91121	8.780	0.390	0.352	5, 7	75	−176	−77	0.70	5673	−1.08	3.88	G1WF2/5 V	
94028	8.227	0.342	0.254	1, 2, 3	−26	−135	18	0.70	5934	−1.39	4.23	F4V	
97320	8.170	0.338	0.301	1, 3	84	−18	−31	0.72	5983	−1.23	4.17	F3V	
99682	8.645	0.342	0.373	4	−65	−15	−8	0.97	6034	−0.45	4.06	F6V	
101976	8.310	0.413	0.315	4	1	27	66	0.95	5554	−0.49	3.87	G1V	
102200	8.740	0.330	0.300	2, 3	100	−136	16	0.76	6037	−1.23	4.13	F2V	
108317	8.036	0.447	0.291	4	−127	−106	−11	0.80[1]	5332	−2.19	2.75	G0	b
111777	8.490	0.395	0.257	2	−109	−82	−39	0.71	5606	−0.85	4.36	G1/G2	
116064	8.807	0.345	0.273	2, 3	−94	−222	120	0.70[2]	5945	−1.88	4.28	sdF0	
120559	7.970	0.423	0.203	1, 2	−18	−43	−29	0.70	5406	−0.99	4.59	G5WF8 V	b
122196	8.736	0.349	0.331	1, 3	−164	−136	20	0.84	5934	−1.69	3.92	sdF5	
124785	8.666	0.388	0.328	1, 3	−29	−105	46	0.86	5694	−0.69	3.86	F8/G0WF5	
126793	8.208	0.367	0.290	1, 3	−4	6	−7	0.80	5800	−0.81	4.18	G0WF3/5	
128279	8.034	0.465	0.268	1, 3	23	−92	−265	0.80[1]	5216	−2.16	2.94	G0	
132475	8.558	0.393	0.283	1, 2, 3	52	−361	61	0.70[2]	5619	−1.53	3.75	F5/F6V	v
140283	7.213	0.380	0.287	1, 2	−238	−248	50	0.77	5751	−2.26	3.71	sdF3	v
142945	8.011	0.389	0.251	1	70	−41	4	0.70	5633	−1.00	4.35	F8V	b
144450	8.084	0.485	0.245	4	−5	−76	22	0.70[3]	5077	−1.17	3.42	G6V	
145417	7.520	0.510	0.170	1, 2	−40	−85	−22	0.60[2]	4908	−1.36	4.69	G8/K0 V(W)	
160617	8.733	0.345	0.335	2, 3	65	−210	−87	0.77	5967	−1.77	3.79	Fw	
166913	8.221	0.327	0.302	1, 3	−41	−40	77	0.72	6065	−1.54	4.13	F6:Vw	
188510	8.834	0.416	0.163	2	−142	−108	70	0.60[2]	5423	−1.62	4.47	G5Vw	b
193901	8.659	0.382	0.219	1, 2	−146	−240	−67	0.70[2]	5657	−1.16	4.46	F7V	
194598	8.354	0.344	0.269	2	−66	−271	−24	0.70	5928	−1.14	4.23	F7V−VI	
196892	8.245	0.349	0.304	1, 2, 3	8	−125	−24	0.78	5912	−1.09	4.11	F6V	b?
196944	8.398	0.449	0.348	1	−142	−131	−15	0.80[1]	5353[4]	−2.23	1.70[4]	G2-5II	Ba, b
199289	8.293	0.363	0.261	1, 2	−31	−62	−18	0.70[2]	5800	−1.10	4.21	F5V	b?
200654	9.097	0.460	0.271	2	−265	−384	−138	0.80[1,3]	5340	−2.99	2.96	G:w	
201891	7.379	0.359	0.254	1, 2, 3	102	−110	−52	0.70	5821	−1.14	4.20	F8V−VI	b?
203608	4.229	0.330	0.317	6	−3	49	13	0.88	6063	−0.74	4.29	F6V	v
211998	5.281	0.451	0.239	1, 2	−160	−144	−68	0.89	5255	−1.49	3.44	A3V?+F9V	b
213467	8.531	0.484	0.288	1	−223	−220	−79	0.80[1,3]	5099	−1.43	2.92	G5VWF3	

[1] Adopted mass $0.80\,M_\odot$. [2] The star is located on the lower side of the track. [3] The star is located where the tracks are very compact. [4] T_{eff}, $\log g$, and ξ_t adopted from Začs et al. (1998).

from sources given in the table caption. The empirical temperature calibration of Alonso et al. (1996; their Eq. (9)) was used to estimate the effective temperatures. This calibration is based on the InfraRed Flux Method, a grid of Kurucz' atmosphere models and a large sample of dwarfs and subdwarfs in the metallicity range $−3 \leq$ [Fe/H] ≤ 0.5. In applying the calibration we iterated until consistency was achieved between the calculated temperatures, the metallicities, the surface gravities and the derived iron abundances of the stars. The effective temperature of the star HD 196944 was adopted from Začs et al. (1998). The reddening was calculated for all stars from H_β, and was found to be small for all stars but one, so reddening was neglected in the analysis (see Sect. 5.2, below).

Metallicities. The overall metallicities, [Me/H], of the stars were first approximated by using a calibration of Strömgren photometry made by Schuster & Nissen. The metallicities were changed until consistency was achieved with the derived iron abundances, [Fe/H], from lines of Fe I, the surface gravities and the effective temperatures.

Surface gravities. Values of $\log g$ were calculated from Hipparcos parallaxes in the same way as described by Nissen et al. (1997) in their Eq. (3). An age of 14 Gyr was assumed for all stars. The stellar masses were estimated from the evolutionary tracks of VandenBerg et al. (2000). For some stars, that were not faint enough for these tracks, $0.80\,M_\odot$ was adopted. Some stars were located on the lower side of the track, and some stars resided in the crowded part of the giant branch. In these cases, the masses will have higher uncertainties. The visual magnitudes were adopted from different sources, the bolometric corrections were determined from Alonso et al. (1995),
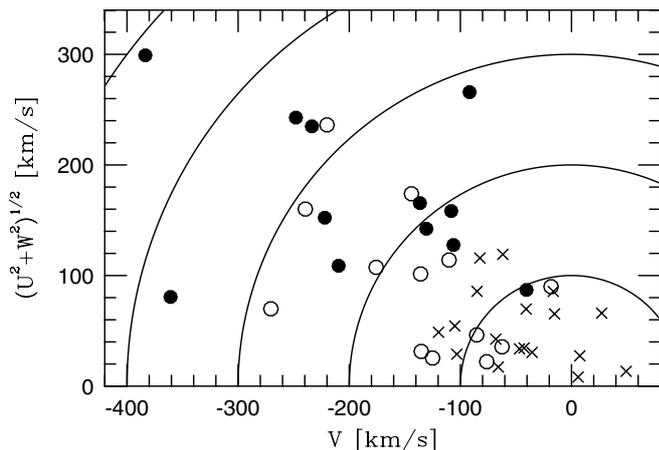
Fig. 2. A Toomre diagram for the stars, where the symbols have been coded according to the overall stellar metallicity: $-1.0 \leq$ [Fe/H] (crosses), $-1.5 \leq$ [Fe/H] < -1.0 (open circles), and [Fe/H] < -1.5 (filled circles). The curves connect loci with identical total velocities relative to the LSR. The diagram shows an obvious anticorrelation between overall metallicity and total LSR velocity.

and the parallaxes adopted from the Hipparcos catalogue (ESA 1997). The temperatures, metallicities, iron abundances, and gravities were iterated until consistency was achieved. The surface gravity of the star HD 196944 was set to $\log g = 1.7$ according to Začs et al. (1998).

Microturbulence parameters. ξ_t represents the doppler broadening of the lines by non-thermal small-scale motions in the stellar atmosphere. Here the microturbulence parameter was set to $\xi_t = 1.5 \, \text{km s}^{-1}$. A microturbulence parameter of $1.9 \, \text{km s}^{-1}$ was adopted from Začs et al. (1998) for the star HD 196944.

3.2. Stellar space velocities

Galactic space velocities U, V and W, in a right-handed system with U directed towards the galactic center, were computed for the programme stars with the transformations given by Johnson & Soderblom (1987). Parallaxes and proper motions were adopted from the Hipparcos catalogue (ESA 1997). Accurate radial velocity data for 39 of our 43 stars were kindly supplied in advance of publication by Birgitta Nordström, Copenhagen (Nordström et al. 2004). For the remaining four stars the radial velocities were obtained from the CDS database (Egret 1986). The resulting velocities relative to the LSR are given in Table 2, where we have used the solar velocities relative to the LSR $U_\odot = +10.00$, $V_\odot = +5.25$ and $W_\odot = +7.17 \, \text{km s}^{-1}$ of Dehnen & Binney (1998).

Figure 2 shows the kinematic Toomre diagram for our sample and displays the well-known relation between overall metallicity and velocity relative to the local standard of rest.

3.3. Abundance analysis

3.3.1. The properties of the analysing program

The Uppsala programme EQWIDTH was used to analyse the measured stellar absorption lines. In this programme LTE is assumed, but a source function is adopted to properly allow for continuum scattering. This is important mainly for UV spectra of metal-poor stars. For a given model atmosphere and for an adequate number of wavelength points, EQWIDTH solves the equation of radiative transfer, integrates an equivalent width, compares with the observed width, and then determines the corresponding abundance by iteration.

The lines chosen were selected to be essentially free of blends. Since most lines are weak both in the solar and stellar spectra, the effects on the equivalent widths by isotope splitting (IS) and hyperfine-structure splitting (hfs) should not be important. The exception may be the Ba II line (at 6141.71 Å), which is blended with a line of Fe I and which shows both hfs and IS. For this line we made detailed synthetic-spectrum calculations with the programme BSYN, a sister programme to EQWIDTH, taking the iron-line blend and the different line components into consideration with hfs and IS data from McWilliam (1998) and assuming solar isotope ratios. We found, however, that the IS and hfs splittings are negligible for this line.

The oxygen IR triplet lines, used here for determining the oxygen abundances, are known to be severely affected by departures from LTE (e.g. Kiselman 1991, 1993; Nissen et al. 2002). We have therefore solved the statistical-equilibrium equations for an oxygen model atom with 23 levels and 65 radiative transitions, kindly provided by Dan Kiselman. For method and atomic data; see Nissen et al. (2002). These calculations were made individually for each star with appropriate model atmospheres. The corrections in abundances range from -0.07 to -0.33 dex and barely seem affected by the uncertainties in hydrogen-collision cross sections (cf. Nissen et al. 2002).

3.3.2. Atomic line data

The Vienna Atomic Line Data Base, VALD (Kupka et al. 1999), was used for gathering atomic line data, such as wavelengths λ, excitation energies χ_{lower}, and radiation damping constants γ_{rad}. For some lines of sodium, magnesium and silicon VALD had no radiation damping constants listed, so they were then taken from the tables of Kurucz (1989). For the barium line the radiation damping constant was calculated from lifetimes of relevant energy levels identified in the tables of Bashkin & Stoner (1975). The line data are given in Table 3 which is only available in electronic form.

3.3.3. Pressure broadening

To deal with collisional broadening induced by neutral hydrogen, we applied the data of Barklem et al. (2000), based on quantum mechanical calculations for 46 of 62 lines. For lines not covered by Barklem et al., the Unsöld (1955) approximation with enhancement factors was adopted. The enhancement

factors applied in this investigation were adopted from the literature: Na I: Holweger (1971), Si I: Holweger (1973), and Fe II: Holweger et al. (1990). For Mg I and Sc II, a value of 2.50 was applied following Mäckle et al. (1975). The different broadening methods are compared in Sect. 5.6.1.

3.3.4. Oscillator strengths

For determining the absolute abundance one needs the product of the statistical weight g and the oscillator strength f for the transition. We performed a differential analysis relative to the Sun and determined astrophysical $\log gf$ values by running the analysis programme EQWIDTH with known abundances, solar-flux equivalent widths, and a solar model atmosphere. The photospheric solar abundances, $\log \epsilon_\odot$ (Table 3), were adopted from Grevesse & Sauval (1998) with the exception of oxygen for which the abundance of Asplund et al. (2004) was adopted. A MARCS model was used with the parameters $T_{\text{eff}} = 5780$ K, $\log g = 4.44$ dex, [Fe/H] $= 0.00$ dex, and $\xi_{\text{t}} = 1.15$ km s^{-1}. For the oxygen triplet lines, corrections for NLTE (-0.22 dex) were applied when determining the gf values.

The choice of a differential analysis relative to the Sun may not be optimal in our case. The stars depart systematically from the Sun in one important respect: they are more metal-poor so their lines from heavy elements are generally weaker. Also, the choice of a MARCS model is not obvious. True enough, errors may cancel if one chooses the Solar model from the same grid as for the programme stars; however, this cancellation may be only partial since, the programme stars are systematically different. Therefore, arguments for adopting a semi-empirical solar model instead can be raised; cf. Sect. 5.6.3.

The solar equivalent widths were measured from a computer-readable version of the atlas of Kurucz et al. (1984). The lines were fitted twice with the programme package IRAF: with a Gaussian fit and alternately by a numerical integration. The final width was set as a weighted mean of these values, with the weighting determined by visual inspection.

When determining the gf value of the Ba II 6141.713 Å line, which has an Fe I blend, we first scaled the iron line gf value to two other lines of the same multiplet, 6232.5 and 6302.5 Å, which were fitted to the solar flux atlas of Kurucz et al. (1984). The relative scaling was based on the gf values listed by Bard et al. (1991), and the fitting of the two lines resulted in increased $\log gf$ values by $+0.02$ and $+0.10$ dex, respectively. The adopted $\log gf$ value of the Fe I is -1.40; 0.06 dex higher than given by Bard et al. Synthesis of the Ba II line, including the (negligible) hfs and IS splittings and the Fe I line to the solar atlas, indicated that the Ba and Fe lines do not differ in central wavelengths by more than 0.005 Å. Therefore these wavelengths were set to be identical. Finally, requiring the total equivalent width of the blend to be equal to our measured solar equivalent width resulted in a $\log gf$ for the Ba II line of -0.13, which is 1.1 σ lower than the NBS value of -0.077 (Wiese & Martin 1980).

4. Results

The results of the abundance analysis are given in Table 4 and displayed in Fig. 3. Here we added the abundances of disk stars, obtained with very similar data and methods. A number of different morphological patterns are shown in the figure, many of which have been found and discussed by others. We recognise the "α-element behaviour" of Mg, Si, Ca, and possibly of Ti, with a rise of [X/Fe] as one proceeds towards the more metal-poor stars, and a levelling off to a plateau for [Fe/H] < -1. It is not clear, however, that this plateau level is strictly horizontal, a question which will be discussed in Sect. 6. Also, O shows similar behaviour. We saw "iron-like" behaviour of Ni and possibly Cr, with [X/Fe] staying close to solar also for metal-poor stars. We found that the "odd-Z element" Al behaves like the even-Z alpha elements (cf. Si!), while the odd Na behaves differently. We find that Sc, V, and Ba do not show any clear rise relative to Fe with decreasing [Fe/H] and that the [Ba/Fe] ratio (based on only one blended feature) shows a substantial scatter, seemingly caused by some pronounced outliers. In all panels of Fig. 3 where our data overlap with the disk star data there is a smooth transition between the data sets.

One important question is if the scatter around the mean trends in Fig. 3 are real or caused by errors in the analysis; e.g., is the increased scatter, when we proceed to stars with [Fe/H] < -1.0, visible for most elements, due to a real spread in abundances or caused by weaker and fewer measurable lines, lower S/N, or more uncertain fundamental parameters? Do the differences in scatter, ranging from 0.03 dex (in [Ca/Fe]) to above 0.1 dex (e.g. in [O/Fe], [Al/Fe], [Ba/Fe]) around the mean relations, tell us anything about nucleosynthesis? Is any of the scatter in the alpha elements [Si/Fe] and [Mg/Fe] real, in view of the smaller scatter in [Ca/Fe] at a given [Fe/H]? Discussion of such questions will be postponed until after both the error discussion in Sect. 5 and a detailed comparison with results from other studies in Sect. 6.

One additional feature of Fig. 3 should be pointed out – the nice agreement in iron abundances as derived from the Fe I lines and the (single!) Fe II line. This agreement will also be further discussed in Sect. 6.

5. Consistency checks and error estimates

5.1. Abundance dependence on individual lines

A check was performed to see if any individual lines of the elements represented by numerous lines in our spectra tend to give systematically different abundances from the rest of the lines. The relative abundances [X/H]$_{\text{line}}-$[X/H]$_{\text{mean}}$ were thus calculated for all iron and nickel lines included in the programme; see Fig. 4. Some lines did give systematically different abundances from the mean abundance of the species, and the Ni line 7788 Å was removed from the abundance determinations altogether. The reason for the deviating abundances from individual lines could be due to hidden blends in the Sun, and therefore erroneous $\log gf$ values, or hidden blends or departures from LTE in the stellar spectra depending on the parameters.

Some silicon lines (6125, 6142, 6145, and 6155 Å) come from double, not single, electron transitions in the atoms. We

Table 4. Spectroscopic metallicities [Fe/H]$_{Fe\,I}$, and abundances relative to iron [X/Fe]$_{Fe\,I}$, derived for 13 neutral and ionized species X. For oxygen, NLTE corrections were applied: $[\alpha/\mathrm{Fe}] = \frac{1}{4}([\mathrm{Mg/Fe}] + [\mathrm{Si/Fe}] + [\mathrm{Ca/Fe}] + [\mathrm{Ti/Fe}])$, and $[\alpha'/\mathrm{Fe}] = \frac{1}{3}([\mathrm{Mg/Fe}] + [\mathrm{Si/Fe}] + [\mathrm{Ca/Fe}])$.

HD	[Fe/H]	O I	Na I	Mg I	Al I	Si I	Ca I	Sc II	Ti I	V I	Cr I	Fe II	Ni I	Ba II	α/α'
17072	−0.98	0.61	−0.12	0.36	0.24	0.32	0.35	−0.08	0.18	−0.10		0.05	−0.10	0.59	0.31/0.34
25704	−0.97	0.54	0.16	0.33	0.32	0.20	0.19		0.06		0.13	−0.01	0.04	−0.24	/0.24
49301	−0.82	0.35	0.21	0.37	0.29	0.22	0.28		0.25	0.17	0.24	−0.17	0.02	0.04	0.28/0.29
59374	−0.93	0.51	0.19	0.39		0.20	0.24		0.20	0.11	0.17	0.05	0.07	−0.26	0.26/0.28
61902	−0.71	0.23	0.10	0.12	0.10	0.11	0.13			0.09	−0.14	0.02	0.03	−0.03	/0.12
63598	−0.84	0.46	0.11	0.31	0.24	0.23	0.22		0.34	0.15	0.03	−0.03	−0.03	−0.19	0.28/0.25
76932	−0.89	0.50	0.11	0.32	0.17	0.24	0.24		0.30	0.15	−0.06	0.01	−0.02	−0.11	0.27/0.27
78747	−0.80	0.62	0.20	0.39	0.33	0.26	0.26		0.21	0.01		0.08	0.05	−0.28	/0.30
79601	−0.74	0.57	0.19	0.39	0.35	0.27	0.22		0.29	0.21	0.01	0.00	0.06	−0.34	0.29/0.29
80863	−0.61	0.46	0.18	0.33	0.27	0.21	0.11		0.17	0.08	0.04	0.04	0.03	−0.27	0.20/0.22
84937	−1.96	0.42	0.12				0.27						−0.44		
91121	−1.08	0.67	0.04	0.41	0.34	0.40	0.26		0.23	0.01	0.15	0.03	−0.04	0.07	0.33/0.36
94028	−1.39	0.56	−0.05	0.30	0.46	0.29	0.23					−0.09	0.06	−0.04	/0.27
97320	−1.23	0.55	0.10	0.31	0.22	0.26	0.23					0.06	0.12	−0.14	/0.27
99682	−0.45	0.23	0.12	0.05	0.03	0.07	0.06			0.00	0.00	0.04	−0.02	0.02	/0.06
101976	−0.49	0.30	0.09	0.14	0.17	0.11	0.07			−0.02	0.01	0.04	−0.05	−0.17	/0.11
102200	−1.23	0.44	−0.07	0.19		0.17	0.20					−0.17	−0.01	−0.14	/0.19
108317	−2.19	0.59	−0.05	0.57		0.21	0.39					0.08		−0.17	/0.39
111777	−0.85	0.59	0.23	0.38	0.35	0.30			0.21		0.03		0.09		
116064	−1.88	0.75	0.02	0.36		−0.04	0.34							−0.32	/0.22
120559	−0.99	0.65	0.15	0.34	0.35	0.25	0.21		0.32	0.25	0.14	0.08	0.04	−0.32	0.28/0.27
122196	−1.69	0.38	−0.18	0.18		−0.11	0.18					−0.05	0.11	−0.29	/0.08
124785	−0.69	0.56	0.22	0.32	0.34	0.29	0.24		0.25	0.09	0.07	0.04	0.05	−0.21	0.27/0.28
126793	−0.81	0.51	0.15	0.33	0.29	0.27	0.18		0.22	0.24	−0.10	−0.01	−0.02	−0.24	0.25/0.26
128279	−2.16	0.77	−0.20	0.42		0.27	0.32					0.09	−0.02	−0.74	/0.34
132475	−1.53	0.76	0.08	0.37	0.25	0.45	0.31		0.17	0.19		0.05	0.09	0.06	0.32/0.38
140283	−2.26	0.69	−0.18	0.10			−0.02							−1.11	
142945	−1.00	0.73	0.11	0.36	0.34	0.31	0.28	0.09	0.42	0.11	0.00	0.08	0.06	−0.14	0.34/0.32
144450	−1.17	0.73	0.04	0.41	0.43	0.42	0.31			0.09	0.08	0.03	0.14	0.00	/0.38
145417	−1.36	0.60	−0.01	0.33	0.16	0.23	0.37	0.13	0.50	0.31	0.16	0.02	−0.09	−0.16	0.36/0.31
160617	−1.77	0.41	0.24	0.32		0.30	0.40					0.05	−0.07	0.01	/0.34
166913	−1.54	0.60	−0.09	0.37		0.35	0.33					−0.04	−0.10	−0.07	/0.35
188510	−1.62	0.68	−0.13	0.28		0.14	0.27	−0.05					−0.10	−0.25	/0.23
193901	−1.16	0.58	−0.20	0.17		0.12	0.17	−0.07				0.08	−0.20	−0.25	/0.15
194598	−1.14	0.45	−0.10	0.30		0.08	0.18	0.06				0.06	−0.21		/0.19
196892	−1.09	0.61	0.02	0.40	0.36	0.34	0.31					0.01	−0.05	0.04	/0.35
196944	−2.23	0.85	0.07	0.38		0.43	0.32	−0.30				−0.11		1.14	/0.38
199289	−1.10	0.60	0.13	0.32	0.29	0.27	0.22		0.29	0.16	−0.09	0.05	0.03	−0.28	0.28/0.27
200654	−2.99			0.64			0.70							−0.73	
201891	−1.14	0.60	0.08	0.30	0.37	0.24	0.19			0.07		0.02	0.03	−0.30	/0.24
203608	−0.74	0.32	0.17	0.17	0.11	0.11	0.10	0.04		0.13	0.00	−0.01	0.01	−0.11	/0.13
211998	−1.49	0.74	−0.16	0.44	0.14	0.31	0.33		0.26	0.19		0.05	−0.05	−0.29	0.34/0.36
213467	−1.43	0.57	−0.19	0.32	0.05	0.29	0.31	0.06		0.03	0.27	0.06	−0.13	−0.03	/0.30

checked whether these lines behaved differently compared to the rest, but they did not differ more than expected statistically.

5.2. Errors in the stellar effective temperatures

The uncorrected $(b - y)$ colours, as well as other uncorrected indices, were used for estimating stellar effective temperatures. This should not affect the result much because the interstellar reddening, derived from the observed $(b-y)$ minus the reddening free $(b - y)_0$ according to Olsen (1988), were found to be negligible for all stars except HD 132475 for which the colour excess was $E(b - y) = 0.034$. This corresponds to an effective temperature error of 180 K. Hakkila et al. (1997) have constructed a model for interstellar reddening in the solar neighbourhood based on published results from large-scale surveys of interstellar extinction. Using that model we found reddenings of typically $E(b - y) = 0.00$ to 0.015 mag, the median value being 0.010. For a few stars we found values extending beyond 0.03 mag, namely HD 126793, 132475, 144450, 160617, 193901, and 196944. The largest values appear for HD 126793 ($E(b - y) = 0.046$), HD 144450 (0.052), and HD 196944 (0.065). For HD 132475 the Hakkila et al. model gives $E(b - y) = 0.025$, i.e. somewhat smaller than the value
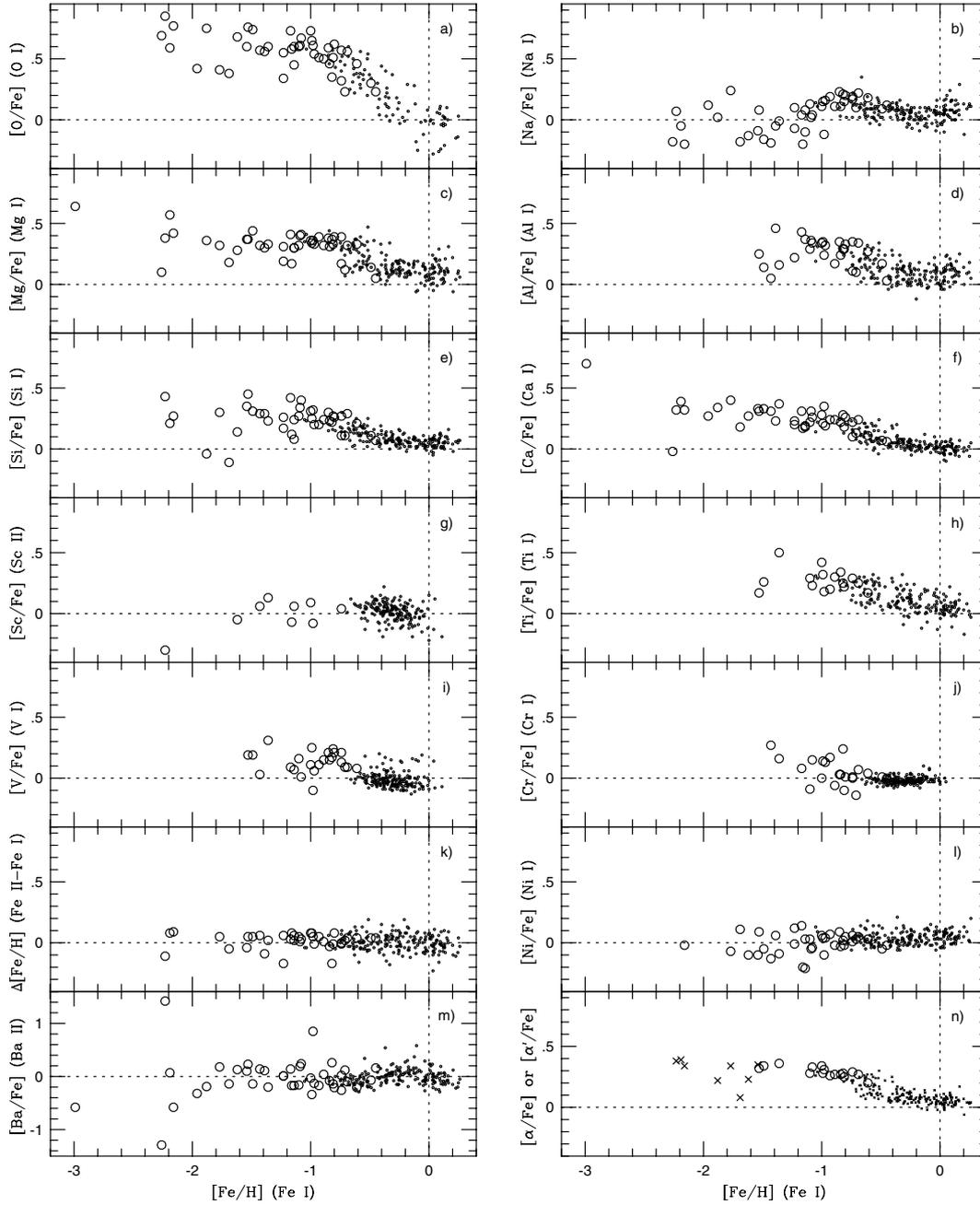
Fig. 3. The abundances relative to iron $[X/\text{Fe}]_{\text{FeI}}$ for all species in the programme as a function of the iron abundance with addition of the data of Edvardsson et al. (1993) as small dots. For species where Edvardsson et al. have no data (Sc I, V I and Cr I) the data of Reddy et al. (2003) is shown instead. Note the different ordinate scale in panel m). In panel n) the circles denote $[\alpha/\text{Fe}] = \frac{1}{4}([\text{Mg/Fe}] + [\text{Si/Fe}] + [\text{Ca/Fe}] + [\text{Ti/Fe}])$, and the crosses $[\alpha'/\text{Fe}] = \frac{1}{3}([\text{Mg/Fe}] + [\text{Si/Fe}] + [\text{Ca/Fe}])$ for stars with no Ti abundance determinations.

from the H_β photometry. However, the mean error in the estimates from the model is typically 0.05 mag. We conclude that reddenings of typically 0.01 mag may affect many of our programme stars, leading to underestimates of effective temperature by about 50 K and of metal abundances of about 0.03 dex. For a few stars like HD 132475, there may be more serious underestimates, by even somewhat more than 0.1 dex.

A test was made to investigate the impact of the temperature errors. Alonso et al. (1996) estimate a standard deviation of 110 K in the effective temperatures. Here the parameters were changed ±100 K for all stars. The changes of the

chemical abundances were at a mean ±0.04 dex, but for O I, Ca I, Ti I, V I, Fe I, and Ba II the mean abundances changed by more than 0.07 dex, see Table 5. Thus, errors in the effective temperatures have considerable impact on the result.

A frequently used consistency test of the effective temperatures is to check if the derived abundances are dependent on the excitation energies for the lower states of the lines. The level populations depend on the temperatures through the Boltzmann distribution in the LTE approximation. The numerous lines of Fe I and Ni I with wide ranges both in excitation energy and equivalent widths were selected for these consistency checks.
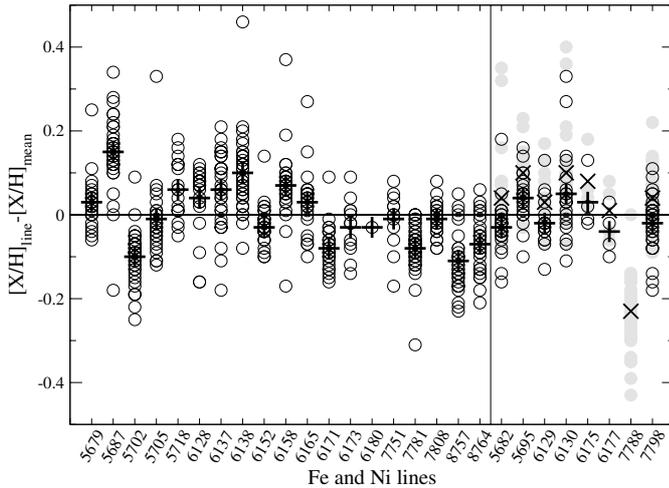
Fig. 4. A consistency check of the abundances of iron (*left*) and nickel (*right*). The open black circles mark the measurements for each line for each star and the thick (+):s mark the mean for individual lines. For nickel the filled grey circles and the thick (**x**):s mark the measurements with the line 7788 Å included. This line was later removed from the analysis due to suspected blending.

The use of both species together was motivated by the similarities between the elements and the gain in statistics with as many lines as possible.

For each star included in the tests a diagram was plotted to display the abundance from each line minus the derived mean abundance for the star, $[X/H]_{line}-[X/H]_{mean}$, versus the excitation energy of the lower level of the line, χ_{lower}; see Fig. 5 top panel. To all diagrams a linear fit was sought, and these slopes were then plotted in a new diagram with the effective temperatures of the stars on the abscissa, see Fig. 6.

The check shows that the test is very dependent on the lines employed in the test. If all lines except Ni I 7788 Å are included, the test suggests that the adopted effective temperatures are about 100 K too low for the stars in the lower temperature region and about 25 K too high at high temperatures (thick black line). However, if lines deviating by more than 0.1 dex from the mean in Fig. 4 are removed (removal of the iron lines at 5687 and 8757 Å), the temperatures of the low-temperature stars seem underestimated by some 20 K, while the warmer stars have their temperatures overestimated by about 120 K (thin black line). If spectral lines deviating by more than 0.05 dex are removed (removal of the iron lines at 5687, 5701, 5717, 6136, 6137, 6157, 6170, 7780, 8757, and 8763 Å), then adopted effective temperatures of the low-temperature stars are about 70 K too high and high temperature stars have temperatures about 130 K too low (thick grey line). The conclusion is that this test, assuming that the LTE approximation is valid, suggests that the errors in temperature are not larger than 150 K. For a few stars the temperatures may, however, be underestimated by even more, due to reddening. More precise conclusions cannot be drawn.

Table 5. The mean abundance effects of changes in effective temperature, surface gravity, metallicity, and microturbulence. The last two columns show the abundance change if the $\log gf$-values were calculated with only the Unsöld approximation, see Sect. 5.6.1 or based on the Holweger & Müller model, see Sect. 5.6.3.

Ion	Mean abundance change for all 43 stars					
	T_{eff}	$\log g$	[Me/H]	ξ_t	$\log gf$	$\log gf$
	+100 K	+0.2	+0.5	+0.5	Unsöld	HM
	−100 K	−0.2	−0.5	−0.5	only	model
O I	−0.08	0.06	0.00	−0.03	−0.01	−0.03
	0.08	−0.06	0.01	0.02		
Na I	0.05	0.00	0.01	−0.01	−0.02	−0.12
	−0.05	0.01	−0.01	0.01		
Mg I	0.04	−0.01	0.02	−0.01	*	−0.11
	−0.04	0.02	−0.02	0.01		
Al I	0.03	−0.01	0.01	−0.01	0.00	−0.09
	−0.03	0.01	−0.01	0.01		
Si I	0.03	0.01	0.02	−0.01	−0.02	−0.09
	−0.02	−0.01	−0.01	0.01		
Ca I	0.06	−0.02	0.02	−0.04	−0.03	−0.15
	−0.07	0.02	−0.03	0.05		
Sc II	0.02	0.08	0.08	−0.01	*	−0.06
	−0.02	−0.08	−0.05	0.02		
Ti I	0.09	0.00	0.00	0.00	0.00	−0.10
	−0.10	0.00	−0.01	0.00		
V I	0.10	0.00	0.01	0.00	0.00	−0.11
	−0.10	0.00	−0.01	0.01		
Cr I	0.05	0.00	0.00	0.00	0.04	−0.10
	−0.06	0.00	0.00	0.01		
Fe I	0.07	0.00	0.02	−0.03	−0.04	−0.15
	−0.07	0.00	−0.02	0.04		
Fe II	−0.01	0.08	0.05	−0.01	*	−0.06
	0.02	−0.07	−0.03	0.02		
Ni I	0.05	0.01	0.02	−0.01	0.02	−0.12
	−0.05	−0.01	−0.02	0.01		
Ba II	0.07	0.03	0.09	−0.20	0.08	−0.15
	−0.06	−0.04	−0.06	0.22		

* These species have only lines calculated with the Unsöld approximation from the start.

5.3. Errors in microturbulence parameters

A test was made to investigate the impact of the microturbulence errors. The parameters were changed $\pm0.5\,\mathrm{km\,s^{-1}}$ for all stars. The average change of the mean abundances were only ∓0.03 dex. An exception was barium, for which the change was ∓0.21 dex.

We also checked if the adopted value of $1.5\,\mathrm{km\,s^{-1}}$ for all stars (except for HD 196944) give consistent results by investigating whether the line strengths, $\log(W_{theo}/\lambda)$, and the relative abundances of the lines, $[X/H]_{line}-[X/H]_{mean}$, are correlated. W_{theo} represents the width the line would have if the mean abundance from all lines is adopted, following Magain (1984). If the assumed microturbulence parameter and the underlying line-formation theory are correct, the relative abundances derived from the individual lines would be independent of line strength.

The test was performed in a way similar to that for the effective temperature; Sect. 5.2. A diagram was plotted for each
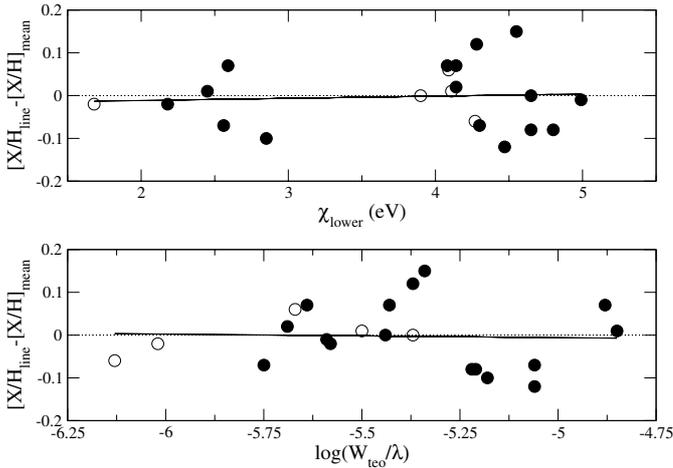
Fig. 5. An example of consistency diagrams for an individual star, in this case HD 126793. Filled circles represent iron lines and open circles nickel lines. Linear fits were made to the data for individual stars, and the derived slopes were studied as functions of stellar parameters, e.g., in Fig. 6.
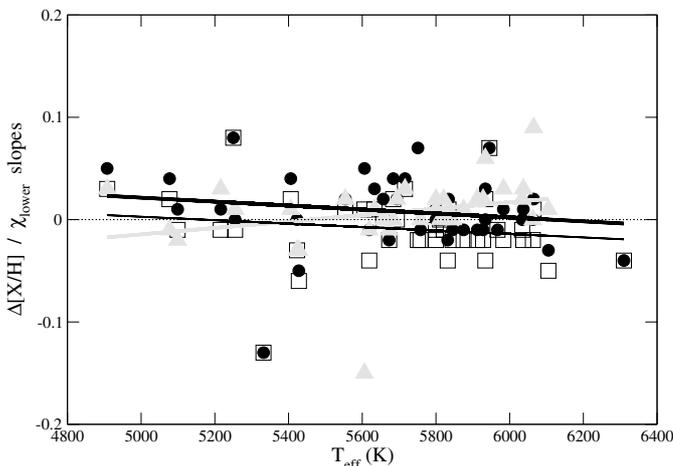

Fig. 6. A consistency check for the effective temperatures. Filled circles and thick black line: all lines included. Squares and black line: the lines 5687 and 8757 Å were removed. Grey triangles and grey line: the lines at 5687, 5701, 5717, 6136, 6137, 6157, 6170, 7780, 8757, and 8763 Å were removed.

star with the relative abundance, $[X/H]_{line}-[X/H]_{mean}$, on the ordinate and the theoretical line strength, $\log(W_{theo}/\lambda)$, on the abscissa, see the lower panel of Fig. 5. To all figures a linear fit was sought.

The results show again that this kind of test is heavily dependent on which lines are included, although one may conclude that the microturbulences are slightly overestimated in general and not optimal for some stars. This has, however, very little impact on the derived mean elemental abundances, with the exception of barium, as discussed in Sect. 6.8.

5.4. Errors in metallicities

In the present study, the iron abundance, [Fe/H], as derived spectroscopically from lines of Fe I, was used to represent the over-all metallicity in the model atmosphere used for the star.
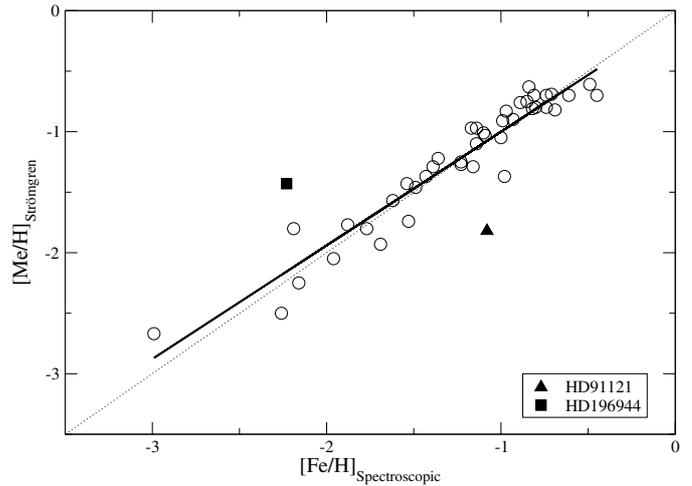
Fig. 7. Comparison of derived iron abundances, [Fe/H], with metallicities from Strömgren photometry obtained from the calibration of Schuster & Nissen (1989). The solid line shows Eq. (2) and the dotted line indicates the 1-to-1 relation.

The effects of errors in the metallicities in the analysis have been tested in the following way:

The metallicities of the model atmospheres were changed ± 0.5 dex for all stars. The change of the mean abundances were on average ± 0.02 dex, but higher for Sc II, Fe II and Ba II, as seen in Table 5. The conclusion is that errors in the metallicities do not have a large impact.

The derived iron abundances are compared with metallicities given by the Schuster & Nissen (1989) calibration of Strömgren photometry in Fig. 7. Note that the correction to Magain's (1987, 1989) [Fe/H] scale was not applied – as this scale was found by Gosset & Magain (1993) to be affected by a non-linear detector. The derived abundances differed from the photometric ones by -0.01 dex on average with a standard deviation of 0.25 dex, a maximum difference of 1.01 dex (HD 91121, with photometry from a separate source) and a minimum difference of -0.58 dex (HD 196944, supergiant). If we remove the 2 outliers, the mean difference does not change and the equation of the black line is

$$[Me/H]_{Stromgren} = -0.06 + 0.94\,[Fe/H]_{Spectroscopic} \qquad (2)$$

with a scatter of 0.15 dex.

5.5. Errors in surface gravities

The gravities derived from Hipparcos parallaxes were estimated as having an average standard deviation error of 0.09 dex. These errors were derived assuming an error of 70 K for the effective temperatures of the stars. For the gravity parameter of the star HD 196944, Začs et al. (1998) claim an error interval of ± 0.3 dex.

Our neglect of interstellar absorption may make our assumed reddening-free V magnitudes too large. Using the result from Sect. 5.2 above, we estimate that typical A_V values hardly exceed 0.04 mag for most stars, and not 0.4 mag for any of them. This corresponds to overestimates in $\log g$ by 0.02
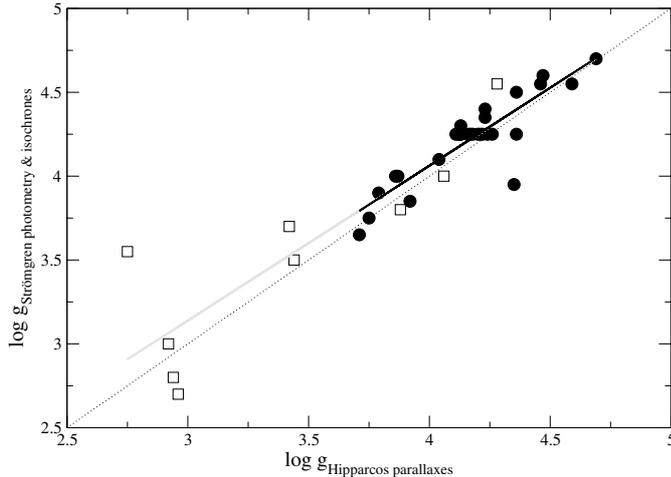
Fig. 8. Comparison between log g from Hipparcos and Strömgren photometry (see text). The filled circles and black line represent stars and fits with reliable data from Strömgren photometry, and squares indicate uncertain measurements. The grey line shows a fit to all data. The dotted line shows the 1-to-1 relation.

to 0.16 dex, respectively. We have compared our gravity estimates with those obtained from Strömgren photometry and the isochrones of VandenBerg & Bell (1985). The results agree very well with those obtained here from the Hipparcos parallaxes. We thus find a relation

$$\log g(\text{isochrones}) = -0.37 + 0.92 \log g(\text{Hipparcos}) \qquad (3)$$

with a standard deviation of 0.18 dex. In fact, if the coolest stars with $\log g < 3.5$ dex are excluded, the standard deviation diminishes to 0.11 dex (cf. Fig. 8). From these considerations, it seems reasonable to adopt an uncertainty on the order of 0.2 dex for our estimates of surface gravity parameters. The effects of these errors on the final element abundances were explored. The change of the elemental abundances were only ±0.02 dex, but for the elements O I, Sc II, Fe II, and Ba II, the changes were larger, from ±0.04 to ±0.08 dex, respectively, see Table 5.

5.6. Errors in the oscillator strengths

5.6.1. Pressure broadening

If the Unsöld approximation with a correction factor was used for all lines when fitting the solar equivalent widths, the log gf values became on the mean 0.03 dex higher with a maximum of +0.26 dex. The mean abundances of the stellar sample changed very little as seen in Table 5, but for stars with few measured lines of some element the effect may be important.

5.6.2. Solar equivalent widths and log *gf* values

The stellar and solar equivalent widths were estimated through a weighted mean of a Gaussian fit and pure integration. With this method the solar equivalent widths became larger than the ones used in the investigation of disk dwarf stars by Edvardsson et al. (1993), who only used Gaussian fits to their lines, and

therefore parts of the line wings were not included. The mean difference was 2.2 mÅ (3.3%), with a maximum of 8.6 mÅ (9.9%). However, Edvardsson et al. systematically used the Unsöld approximation while our application of the O'Mara, Anstee & Barklem data lower the resulting log gf values, counteracting the effects of our higher solar equivalent widths. Except for the O I triplet lines, for which Edvardsson et al. did not make any NLTE corrections, the mean difference in log gf (us−Edvardsson et al.) is 0.02 dex with a standard deviation of 0.05 dex for the 28 lines in common.

The error in the gf values deduced for the blended Ba II line at 6141 Å depends on the strength adopted for the blending Fe I line. If the latter line is totally neglected, we find that the gf value for the Ba II line increases to $\log gf = 0.09$, and the typical Ba abundances for the programme stars decrease by 0.15 dex. An increase of the gf value of the Fe I line by 0.2 dex cannot be excluded, which leads to $\log gf(\text{Ba II}) = -0.30$, and to a typical increase of the Ba abundances by 0.13 dex.

5.6.3. Astrophysical log *gf*'s from the Holweger-Müller model

As an alternative to the MARCS model, the Holweger & Müller (1974) model (HM) was used in a test to derive astrophysical log gf values for the lines in the programme. The log gf values then became 0.11 dex higher on the mean compared to the ones from a MARCS solar model, with a maximum difference of +0.20 dex. The stellar abundances decreased by 0.03 dex to 0.15 dex, with a mean of 0.10 dex for all species, see Table 5.

Although we chose a strictly differential approach in this work, with a solar model from the same grid as the model atmospheres representing the stars, this choice was not obvious, see Sect. 3.3.4. The HM model is known to represent solar limb-darkening and fluxes quite well, and in fact more successfully than theoretical flux-constant 1D models (cf. Blackwell et al. 1995; Gehren et al. 2001; Edvardsson et al., in preparation). Thus, there are reasons to believe that the gf values derived from that model might be better in absolute terms. The cancellation argument, founded on the expectation that systematic errors in the stellar model atmospheres act in similar ways in the solar analysis, is of uncertain weight. Thus, systematic errors in abundances [X/H] of about 0.15 dex are possible. The corresponding errors in abundances relative to iron are smaller; [X/Fe] are on the mean 0.05 dex higher when derived with the HM model (oxygen not included).

5.6.4. log *gf*'s from VALD

The analysis was also alternatively performed using oscillator strengths taken from the VALD database. The log gf values from VALD were on average only 0.04 dex lower compared to the ones used in the programme, but the maximum difference (us-VALD) was as large as 2.15 dex (the Fe I line 7780.552 Å) and the minimum −0.60 dex. The difference (us-VALD) for neutral iron alone was on the mean −0.48 dex, with a spread as large as 0.99 dex. This of course had a large impact on the abundances derived, especially for species measured with only

one line. A larger spread and sometimes a different form of the abundance trends in the diagrams could be seen. We believe that although the use of astrophysical $\log gf$ values has drawbacks – they depend on the solar model atmosphere, the damping, and on errors introduced in the measurement of equivalent widths – they are still to be preferred in a differential analysis.

5.7. Binaries

If a star is a binary the absolute magnitude and radius determination will be affected and the surface gravity, $\log g$, will be underestimated. The error in the $\log g$ may amount to 0.3 dex. Also, there may be some error in the adopted effective temperature, as well as in the metallicity. None of our spectra show line doubling, which would be an obvious reason for exclusion from the sample. We estimate that the abundances for only a few stars should be significantly affected with abundance errors in excess of 0.05 dex as a result of binarity.

5.8. Errors in the stellar space velocities

The uncertainties in the total space velocities, $V_{tot} = \sqrt{U^2 + V^2 + W^2}$, are estimated to be less than 20 km s^{-1} for all but ten stars which all have V velocities lagging behind the LSR by more than 90 km s^{-1}, V_{tot} larger than 160 km s^{-1}, and metallicities less than [Fe/H] = −1.2. Another seven stars have uncertainties between 10 and 20 km s^{-1}. The major source of these errors is uncertain parallax values, while the radial-velocity errors are negligible.

5.9. Total errors

It is a difficult task to estimate the total errors in abundance analyses, since estimates of different types of errors have to be made and added into simple numbers. From Table 5 we see that the errors in effective temperature are significant for abundances that were derived from atomic lines of elements that are strongly ionized, i.e. Fe, Na, Mg, Al, Si, Ca, Ti, V, Cr, and Ni. For all these elements the errors caused by uncertainties in stellar fundamental parameters are dominated by the effective-temperature uncertainty, and amount to typically 0.05–0.10 dex. In addition to this, errors in gf values as reflected by differences that result from using different solar models may contribute systematic errors of typically 0.1 dex in absolute abundances. To this comes the fact that departures from LTE and convectively generated thermal inhomogeneities may well add systematic errors of typically 0.1 dex or somewhat more (Asplund et al. 2004; Gehren et al. 2004). The errors in abundance ratios, such as [Ca/Fe] are hopefully significantly smaller. For the abundance of Sc, the gravity uncertainty is also significant and may amount to 0.06 dex or so, but a more significant uncertainty for this element is that its abundance is based just on one spectral line and thus measurement errors or blends may be significant. Also the Ba abundance is based on a single and even blended line with an uncertain gf value; in this case the uncertainty in microturbulence parameter is also

significant, and the Ba abundance may therefore well be wrong by 0.3 dex.

A special case is oxygen. Here, effective-temperature errors and errors in the gravity may possibly add up to about 0.15 dex. Since the temperature scale may be systematically in error, this may lead to systematically erroneous abundances by, say, 0.1 dex. In addition to that, there may be errors caused by oversimplified model atmospheres, notably the assumption of plane-parallel stratification. We note that García Pérez et al. (2005) find systematic deviations for metal-poor subdwarfs between abundances from O I triplet lines and [O I] lines of typically 0.2 dex and ascribe these differences to errors in the abundances derived from the triplet lines.

6. Comparisons with previous results

In Fig. 3 we display our results together with abundances for disk stars analysed with very similar data and methods. A general observation is that the transitions between the disk and halo population data are smooth and continuous for all elements.

We have compared our results with those of a number of recent studies which have some stars in common with ours. The results of these comparisons are displayed in Table 6. Although these studies all share a number of basic features (basically similar model assumptions), they deviate partly in terms of details, such as temperature calibrations, gf values, and model atmospheres. We therefore note with satisfaction that the mutual agreement for stars in common is good. We shall now comment more specifically on our results as compared with those of others.

6.1. Iron

Our abundances of iron were based on Fe I lines, in spite of the fact that these may be subject to NLTE effects, due to either over-ionisation (e.g. Saxner & Hammarbäck 1985; Thévenin & Idiart 1999) or departures from LTE excitation (Magain & Zhao 1996). The reason for this choice was simply that just one Fe II line was observed. This line, however, could be measured in all but six stars. The resulting iron abundances were close to those measured from the Fe I lines, the mean difference being +0.03 dex with a standard deviation of 0.07 dex. This result, of a practically null difference, agrees with the finding by Gratton et al. (2003a) and Jehin et al. (1999) and departs significantly from the result of the calculations by Thévenin & Idiart, who find effects ranging from 0.15 dex to 0.3 dex for the range in metallicity of our stars. We note, however, that our result depends on the gf values adopted – if instead of the solar MARCS model, we use the HM model for the Sun, we derive typical over-ionization effects in [Fe II/Fe I] of 0.1 dex for the programme stars.

As is clear from Sect. 5.4 above, we find little evidence of departures from the Boltzmann excitation equilibrium, in contrast with the empirical results of Magain & Zhao (1996), who adopted gf values for the lower excitation iron lines from Blackwell et al. (1995). For the higher excitation lines, however, they derive gf values from fitting observed solar-disk

Table 6. Comparison between our abundance results and those of others for stars in common, including the numbers of stars, the mean differences, and standard deviations. Sources: B: Burris et al. (2000), BG: Baumüller & Gehren (1997), F: Fuhrmann (1998), Ge: Gehren et al. (2004), Gr: Gratton et al. (2003a), J: Jehin et al. (1999), MG: Mashonkina & Gehren (2001), McW: McWilliam (1998), N: Nissen et al. (2002), NS: Nissen & Schuster (1997).

Element	Source	N	$\Delta[X/Y]$(us-Source)
[Fe/H] Fe I	Gr	17	0.02 ± 0.13
	Gr	1	-0.02 ± 0.08
	J	13	-0.03 ± 0.04
	N	8	0.01 ± 0.07
[Fe/H] Fe II	N	6	0.00 ± 0.04
[O/Fe]	B[2]	5	0.05 ± 0.19
	B[3]	5	-0.02 ± 0.15
	Gr	15	0.00 ± 0.12
	N[4]	2	0.01 ± 0.02
	NS	3	0.26 ± 0.06
[Na/Fe]	Gr	5	0.03 ± 0.11
	Ge[6]	4	-0.10 ± 0.06
	NS	3	0.03 ± 0.03
[Al/Fe]	BG	3	-0.14 ± 0.13
[Mg/Fe]	Gr	7	-0.06 ± 0.07
	Ge[6]	4	-0.03 ± 0.12
	F	2	-0.05 ± 0.06
	J	12	0.05 ± 0.06
	NS	3	0.05 ± 0.04
[Si/Fe]	Gr	8	-0.04 ± 0.06
	NS	3	0.05 ± 0.01
[Ca/Fe]	Gr	9	-0.04 ± 0.04
	J	13	0.04 ± 0.04
	NS	3	0.04 ± 0.01
[Sc/Fe]	Gr	4	0.11 ± 0.05
[Ti/Fe]	Gr	6	0.05 ± 0.05
	J	4	0.05 ± 0.04
	NS	2	0.10 ± 0.02
[V/Fe]	Gr	8	0.13 ± 0.13
	J	9	0.19 ± 0.06
[Cr/Fe]	Gr	5	0.15 ± 0.11
	J	8	0.09 ± 0.09
	NS	3	0.07 ± 0.12
[Ni/Fe]	Gr	14	0.01 ± 0.08
	J	13	0.09 ± 0.06
	NS	3	0.01 ± 0.03
[Ba/Fe]	B	2	-0.25 ± 0.37
	J	12	-0.16 ± 0.15
	MG	2	-0.20 ± 0.11
	McW	2	0.14 ± 0.18
	NS	3	-0.05 ± 0.08

[1] HD 140283 ($\Delta = 0.35$), HD 84937 ($\Delta = 0.22$ dex) excluded.

[2] T_{eff} scale according to King (1993).

[3] T_{eff} scale according to Carney (1983).

[4] [O/H] (NLTE) from IR triplet lines.

[5] HD 84937 ($\Delta = 0.53$) excluded.

[6] LTE abundances.

[7] HD 94028, 132475, 140284 ($\Delta = 0.19 - 0.3$) excluded.

[8] HD 116064 ($\Delta = -0.28$) excluded.

[9] HD 84937 ($\Delta = -0.17$), HD 140283 ($\Delta = -0.38$) excluded.
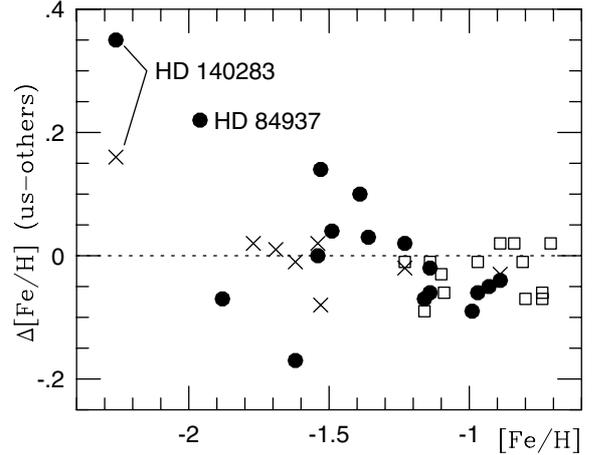
Fig. 9. Comparison of iron abundances derived from Fe I lines with those of Jehin et al. (1999) (squares) and Gratton et al. (2003a) (dots). The differences relative to abundances from lines of Fe II of Nissen et al. (2002) are shown by crosses.

centre equivalent widths to the HM model, adopting a relatively high solar abundance ($\log \epsilon_\odot$(Fe) = 7.68). As these authors note, a systematic lowering of the solar abundance of iron to a value around 7.5, as we have chosen, would nearly cancel their excitation-equilibrium effect for the metal-poor stars, while consistency with a standard LTE analysis with the HM model would not be obtained.

As may be seen from Table 6 and Fig. 9, we find overall agreement in iron abundances with Nissen et al. (2002), Gratton et al. (2003a), and Jehin et al. (1999). The abundances of Nissen et al. were based on about 10 Fe II lines, while those of Gratton et al. are, at least to a great extent, based on Fe I lines. The star with the largest departure by far in the comparison with Gratton et al. is HD 140283, for which we find considerably higher effective temperature, which explains parts of the difference. The second largest departure occurs for HD 84937, the hottest star in our sample.

Jehin et al. (1999) used Fe I lines to derive [Fe/H] abundances differentially relative to HD 76932, for which a metallicity of [Fe/H] = –0.91 was derived from laboratory gf values (our value for this star is −0.89). They also derived iron abundances from Fe II lines; for the 13 stars we have in common their mean value of [Fe/H] from Fe II is −0.02 dex lower than that obtained from the Fe I lines, i.e. no signs of over-ionisation, also consistent with our result.

We also have 13 stars (to some extent the same stars as in the Jehin et al. study) in common with the earlier study of Zhao & Magain (1991). Our values of [Fe/H] depart systematically from those of Zhao & Magain by, on the mean, as much as +0.19 dex. This difference may be ascribed to the choice of gf values and solar iron abundance of Zhao & Magain; they use the HM model to derive gf values for the higher excitation lines and adopt a solar iron abundance, $\log \epsilon$(Fe), of 7.66. Differences between the results of the studies by Zhao & Magain (1991) and Jehin et al. (1999) reflect a basic uncertainty in the solar analysis of iron.
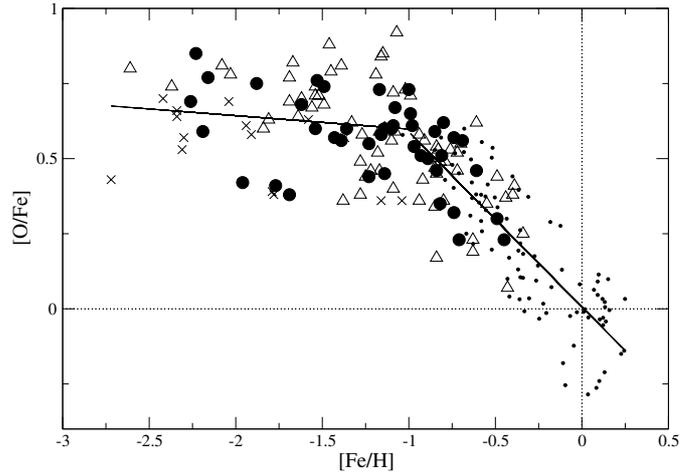
6.2. Oxygen

Our oxygen abundances, as plotted in the [O/Fe] vs. [Fe/H] diagram depart to some extent from the studies of Boesgaard et al. (1999) and Israelian et al. (1998). These authors estimated the oxygen abundances in metal-poor stars from OH lines in the ultraviolet region and found a tendency to systematically increasing [O/Fe] with decreasing [Fe/H], with [O/Fe] values approaching +1.0 for the most metal-poor stars with [Fe/H] around −3. Here, we shall not comment further on the OH oxygen-abundance determinations, which may be severely plagued by uncertainties in UV opacities, convective inhomogeneities, etc. (Asplund et al. 1999; Nissen et al. 2002; Asplund & García Pérez 2001). Boesgaard et al. also made a literature study of the abundances from the oxygen triplet of their programme stars and applied two different temperature scales due to Carney (1983) and King (1993), respectively. There are some differences in our analyses of triplet lines and those of Boesgaard et al. A major difference is that we correct for NLTE effects, which Boesgaard et al. do not. They used a higher oxygen abundance for the Sun than we do, but this is compensated for by our higher gf values. They also use Kurucz models, while we use MARCS models. Boesgaard et al. investigated the difference between the two stellar model grids and concluded that the abundances are 0.07 ± 0.03 dex higher when the Kurucz models are used than for MARCS models, which agrees with our own estimates. Also, there are differences in stellar parameters. For the five stars in common between the two studies our temperatures are on average 47 ± 73 K lower than the King temperature scale, and 85 ± 67 K higher than the Carney scale. Our gravity parameters and metallicities are very similar, as are the observed equivalent widths.

Here we first compare the result of the LTE analyses. For the 5 stars shared with Boesgaard et al. (B), the mean difference [O/H]$_{LTE}$(us–B) is −0.02 with a scatter (s.d.) of ±0.17 dex for the King temperature scale, and −0.09±0.13 dex for the Carney scale. The different stellar models, in addition to the different temperature scales, are the most important reason for the differences in LTE abundances from the oxygen triplet lines.

When we compare our [O/H] abundances from the triplet lines, as corrected for NLTE effects (for the Sun as well as for the stars), they again agree well on average with those of Boesgaard et al. (Table 6).

Gratton et al. (2003a) also published oxygen abundances for Pop II stars based on the triplet lines and calculated corrections for NLTE effects. These authors claim that the resulting corrections are consistent with those calculated by Nissen et al. (2002), so that they ought also to be consistent with our corrections. We find an overall fair agreement with the results of Gratton et al. (Fig. 10 and Table 6). As will be commented on below, the scatter (0.12 dex) for the stars in common may be due to errors in equivalent widths. We note in passing, however, that Gratton et al. derive an oxygen abundance 0.12 ± 0.04 dex higher from the triplet lines than they obtain from the forbidden 6300 Å line, an effect which they ascribe to reddening and binarity, which should affect the triplet lines more than the forbidden one.

Fig. 10. Our oxygen abundances relative to iron, based on the strength of the IR 7774 Å triplet, and with corrections for NLTE applied (filled circles). The values derived with a very similar method by Nissen et al. (2002) are represented by crosses, and those of Gratton et al. (2003a) by triangles. The disk-star data of Edvardsson et al. (1993) (which were empirically normalized to NLTE via the [O I] 6300 Å line) is shown as small dots. The lines are the linear least-squares fits of Eq. (5).

Nissen et al. (2002) have derived oxygen abundances from the triplet lines and alternatively from the forbidden 6300 Å line. NLTE corrections for the triplet lines were applied which are fully consistent with ours. Nissen & Schuster (1997) obtained oxygen abundances from the triplet lines in an LTE analysis, however, differentially versus two Pop II dwarfs with O abundances derived on a scale based on the forbidden lines. Since their range in parameters was rather limited, the authors argue that most of the NLTE effects of the resulting oxygen abundances from the triplet lines should be compensated for. While we find a good agreement for the stars in common with Nissen et al. (2002), the comparison with Nissen & Schuster (1997) shows a mean difference of 0.26 dex and a scatter of 0.06 for the 3 stars in common. When comparing [O/Fe] values by Nissen & Schuster with those derived from the forbidden line of Nissen et al. (2002), we note that the latter values are systematically higher by 0.13 dex. We conclude that the [O/Fe] scale of Nissen & Schuster (1997) seems to be somewhat lower than that of Nissen et al., as well as for the present study. A reason for this may be that the assumed [O/Fe] = 0.30 for the standard stars of Nissen & Schuster departs from that of Nissen et al.; for one of these stars (HD 76932) Nissen et al. (2002) give the value [O/Fe] = 0.44, while our value is 0.38.

In Fig. 10 we plotted our values of [O/Fe] vs. [Fe/H] and compared them to all stars with triplet abundances in the samples of Gratton et al. (2003a) and of Nissen et al. (2002). As expected from the agreement for stars in common we find a general good agreement. Our total equivalent widths for the triplet lines show a scatter relative to the widths of Gratton et al. (2003a) for the stars in common by about 20%, leading to an abundance scatter of about 0.12 dex. It is unlikely, however, that all the scatter in Fig. 10 at a given [Fe/H] is due to errors in equivalent widths. The oxygen triplet lines are very

sensitive to errors in effective temperature and gravity. Errors assumed to be about 100 K in T_{eff} and 0.15 dex in $\log g$ lead to errors in [O/H] of typically 0.1 dex. Although there may be errors in model atmospheres and NLTE corrections that vary systematically with the T_{eff}, $\log g$, and [Fe/H] and cause systematic errors in the oxygen abundances, it is questionable whether these are able to increase the scatter to that observed in Fig. 10. In particular we note three stars, HD 84937, HD 122196, and HD 160617, with [Fe/H] ~ -2 which seem to have lower [O/Fe] values than other stars at these metallicities. Of these stars HD 84937 has the highest positive U velocity of all stars in the sample. HD 160617 was also observed by Nissen et al. (2002) and found to have a comparatively low oxygen abundance.

In order to trace tendencies related to [Fe/H] we also plotted points representing the disk stars analysed by Edvardsson et al. (1993) in Fig. 10. It is seen that the slope for the disk is not clearly broken by a constant plateau with constant [O/Fe] at [Fe/H] ~ -1, as suggested by e.g. Barbuy (1988). Our data instead support a tendency for a continued, although much less steep, gradient towards lower metallicities than that suggested by Israelian et al. (1998) and Boesgaard et al. (1999) on the basis of measurements of OH lines in the ultraviolet. From fits to our data (filled circles) and those of Edvardsson et al. (small dots) we obtain the following mean linear relations for the regions below and above [Fe/H] $= -1.0$:

$-2.75 <$ [Fe/H] < -1.0:

   [O/Fe] $= 0.52 - 0.06$ [Fe/H], $\sigma_{\mathrm{std}} = 0.12$

   $-1.0 <$ [Fe/H] < 0.25:

   [O/Fe] $= 0.00 - 0.60$ [Fe/H], $\sigma_{\mathrm{std}} = 0.12$,   (4)

where σ_{std} denotes the standard deviation of [O/Fe] from the line. The uncertainties in the slope coefficients for the two lines are, respectively, 0.06 and 0.03. When also including the data from Nissen et al. (2002) (diamonds) and Gratton et al. (2003a) (triangles), the fits remain quite similar:

$-2.75 <$ [Fe/H] < -1.0:

   [O/Fe] $= 0.55 - 0.04$ [Fe/H], $\sigma_{\mathrm{std}} = 0.14$

   $-1.0 <$ [Fe/H] < 0.25:

   [O/Fe] $= 0.01 - 0.58$ [Fe/H], $\sigma_{\mathrm{std}} = 0.12$.   (5)

Here the uncertainties in the slope coefficients are 0.04 and 0.03, respectively. We note that our results are consistent with e.g. Barbuy (1988) in that no significant systematic variation of [O/Fe] with [Fe/H] among halo stars is found.

Finally, we note that García Pérez et al. (2005) have recently determined oxygen abundances for Pop II subgiants, for which three different oxygen-abundance criteria have been possible to measure: the IR triplet O I lines, the forbidden 6300.3 Å line, and the OH UV molecular lines. For the most metal-poor subgiants there seems to be a tendency for the triplet lines to indicate higher O abundances than the other criteria, which is contrary to the effect found by Boesgaard et al. (1999) for hotter stars. This effect is not fully understood, but should be taken as a warning that our oxygen abundances may still suffer from systematic errors.
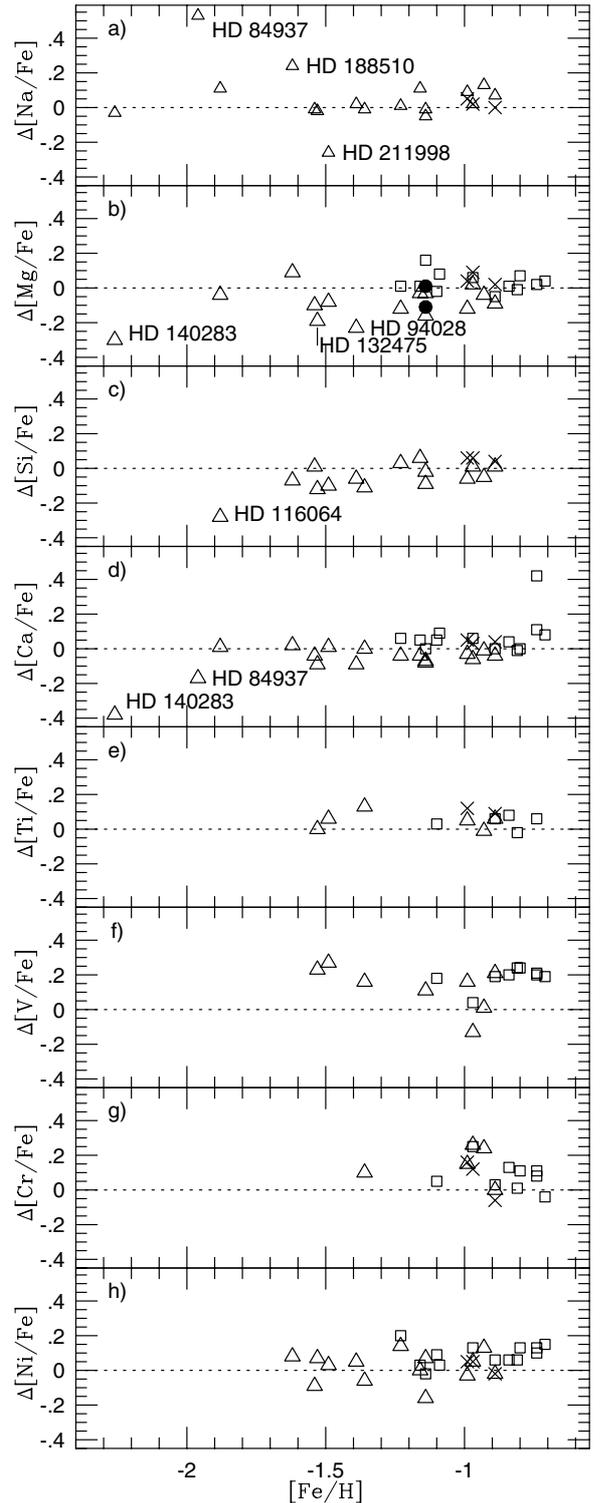
Fig. 11. Comparison of our derived values of [X/Fe] with those of Nissen & Schuster (1997) (crosses), Fuhrmann (1998), (filled circles), Jehin et al. (1999) (squares), and Gratton et al. (2003a) (triangles). Δ[X/Fe] $=$ [X/Fe](us)$-$[X/Fe](others).

6.3. Sodium

Our resulting [Na/Fe] are compared with those of Gratton et al. (2003) and Nissen & Schuster (1997) in Table 6 and Fig. 11 a. Except for three outliers, there is a good agreement. HD 84937

is one of the 3 stars in the full sample (150 stars) of Gratton et al. for which the authors give a value of [Na/Fe] below −0.40, so we recommend a closer inspection of the spectra of this star.

Our [Na/Fe] values are typically about +0.2 for stars around [Fe/H] = −0.8, a value that agrees with the results for the disk by Edvardsson et al. (1993) (see Fig. 3b) and that may be typical both for thin and thick disk stars (Bensby et al. 2003). At lower metallicities, however, [Na/Fe] decreases to 0.0 or close to that, which agrees with the result of McWilliam et al. (1995) for even more metal-poor stars. Baumüller et al. (1998) have studied the NLTE effects on Na abundances for metal-poor stars, and found abundance corrections of typically −0.07 dex for abundances derived from the 5682/88 Å doublet and about half of that from the 6154/60 Å doublet for stars in our parameter range. The effects on the corresponding line in the solar spectrum were found to be marginal. The effects on our most metal-poor stars may be somewhat larger, though probably not very important. Gehren et al. (2004) have recently recalculated their non-LTE corrections for abundances of Na, Al, and Mg for metal-poor stars, with better representations of atoms and of UV fluxes. We note that the [Na/Fe] values for our most metal-poor stars are significantly higher by about 0.2 dex than the NLTE values in Gehren et al. (2004) for their most metal-poor stars, which certainly is a result of their correction for NLTE. For the four stars we have in common, the mean difference between us and Gehren et al. is thus +0.17 dex; if the LTE values of Gehren et al. are compared with ours, the mean difference is instead −0.10 dex according to Table 6.

6.4. Aluminium

For disk metallicities ([Fe/H] ≳ −1.0) our data smoothly join the trend of Edvardsson et al. (1993) in Fig. 3d. At lower metallicities, however, the trend in [Al/Fe] with [Fe/H] found by us is not consistent with the trends found repeatedly by others for field stars (e.g. Aller & Greenstein 1960; Arpigny & Magain 1983; Spite & Spite 1980; Gratton & Sneden 1988; Shetrone 1996), which find systematically decreasing [Al/Fe] with decreasing metallicity with values of [Al/Fe] close to 0.0 at [Fe/H] ∼ −1.5. The situation was summarised by McWilliam (1997). The tendency found by these authors is generally interpreted as a result of the metallicity dependent Al yields predicted for carbon burning by Arnett (1971), although a similar prediction that Na should also decrease with metallicity has not been verified. Even though a tendency toward decreasing Al may be traced in Fig. 3 for the lowest metallicities, our results depart so much from the previous results that it is important to find the reason for the differences. The authors mentioned have no stars directly overlapping with those of our sample for which Al has been determined. While most of the previous authors have used the ultraviolet resonance lines of Al, we used two infrared lines with 4 eV excitation energies (an exception is the work by Shetrone 1996, who, however, analysed Pop II giant stars). Baumüller & Gehren (1997) have performed statistical-equilibrium calculations for Al in Pop II stars. They find very severe effects on the resonance lines, and suggest abundance revisions upwards for determinations from

these lines of 0.4–0.6 dex for solar-type Pop II stars. For the high-excitation lines corrections are much smaller on the order of 0.1 dex. With such corrections applied, our values will be fairly consistent with corrected values from the literature. The calculations of Baumüller & Gehren still suffer from uncertainties in collision cross sections, not the least for collisions with hydrogen atoms. In fact, for the three stars we share, we find a mean difference of −0.14 (cf. Table 6) suggesting that their NLTE effects are somewhat overestimated; for these stars, the BG determinations are based on the near-UV resonance lines. In comparing our results with those of Gehren et al. (2004) we note that our few stars with −1.6 ≤ [Fe/H] ≤ −1.0 tend to lie above their few stars by Δ[Al/Fe] ∼ 0.2 dex. Our results support, however, their main conclusion about the significance of departures from LTE, although problems may remain in fitting the results from models of galactic nucleosynthesis by Timmes et al. (1995).

6.5. Magnesium, silicon and calcium

In general we find a good agreement with Gratton et al. (2003a), Jehin et al. (1999), and Nissen & Schuster (1997) as regards [Mg/Fe], [Si/Fe], and [Ca/Fe] for the common stars (cf. Table 6, Fig. 11b, c and d). For three outliers, however, Gratton et al. give [Mg/Fe] values in excess of ours by 0.19–0.3 dex. These differences basically reflect differences in [Fe/H]; if we compare [Mg/H] values instead, the 3 stars agree well with differences ranging from −0.13 to +0.05, and a mean of −0.06 dex. The agreement in Mg for stars in common with Nissen & Schuster (1997) and Jehin et al. (1999) is good, although their abundances are based on measurements of one single line. Unfortunately, we have only 2 stars in common with the detailed study of Fuhrmann (1998).

Gehren et al. (2004) have found relatively limited but significant NLTE corrections upwards for their Mg abundances of nearby metal-poor stars. Typically, the increase in [Mg/Fe] is 0.1–0.2 dex for their most metal-poor stars. We have four stars in common with their study, and find a mean difference Δ [Mg/Fe](us − Gehren) of −0.16 dex; adopting the LTE values of Gehren et al., we would have obtained −0.03 dex instead.

We note that the NLTE corrections calculated by Gehren et al. are metallicity dependent – from their Table 3 we derive Δ(NLTE-LTE) ∼ −0.07· [Fe/H]. If this correction is applied to the points in Fig. 3, a slowly sloping trend in [Mg/Fe] for stars with [Fe/H] ≤ −1.0 seems to emerge. Such a trend may also be present for the smaller numbers of stars in Gehren et al. (2004), see the middle right panel of their Fig. 6.

For the Si abundances of stars shared with Gratton et al. (2003a) we also find a limited mean deviation and a relatively small scatter, provided that the single outlier is excluded. For stars in common with Nissen & Schuster (1997) we also find good agreement.

Similarly, for the stars with Ca abundances in common with Gratton et al. (2003a) we find good agreement, if two outliers with significantly smaller [Ca/Fe] values in our study are excluded. Again, both these stars deviate due to the differences in [Fe/H], not in [Ca/H] for which they only deviate by 0.05 dex

or less. If all common stars are included, the mean difference in [Ca/H] is −0.03 with a scatter of 0.07. For stars in common with Jehin et al. (1999) and with Nissen & Schuster (1997), we also find only small deviations.

In spite of the relatively marginal differences in abundances between the different studies, we observe some suspicious regularities. The Gratton et al. values of [Mg/Fe], [Si/Fe] and [Ca/Fe] all tend to be higher than ours by, at the most, 0.06 dex, while the Nissen & Schuster values as well as the Jehin et al. values are below ours by about the same amount. Some of these differences may be due to different choices of stellar fundamental parameters or model atmospheres, or else of spectral lines. It seems clear that even if one disregards errors due to 1D LTE model atmospheres with mixing-length convection, realistic systematic errors in abundance analyses for Mg and Si in Pop II stars have this order of magnitude, while they may be smaller for the spectroscopically more ideal element Ca. The trends and scatter for [Mg, Si, Ca/Fe] will be discussed in Sect. 7.2.

6.6. Scandium, titanium, vanadium and chromium

The elements Sc, V, and Cr are represented by just one spectral feature each, and Ti is represented by 2 lines in our study. Also, the number of spectra in which the features could be measured was limited.

As seen in Table 4, abundances from the single Sc II line were only obtained for 9 stars. The results indicate an iron-like behaviour; i.e., with [Sc/Fe] ∼ 0.0, except for the most metal-poor star HD 196944 for which a lower Sc abundance is suggested, Fig. 3. The slowly rising trend in [Sc/Fe] with decreasing metallicity that may be traced in the study of disk stars by Reddy et al. (2003, their Fig. 10) does not seem to continue for Pop II stars. This result departs from the early result of Magain (1989, his Fig. 9) but agrees with the more recent compilation of Norris et al. (2001, their Fig. 8). The general behaviour also agrees with e.g. Cayrel et al. (2004) and Barklem et al. (2005), extending to the most metal-poor stars with a remarkably small scatter. However, we note that both Cayrel et al. and Barklem et al. find a mean [Sc/Fe] somewhat above 0.0, as in fact Norris, Ryan & Beers also suggested for the most metal-poor stars. Our result agrees with the general result of Gratton et al. (2003a), although a direct comparison for the 4 stars in common shows that our values are higher by 0.11 dex on the mean (cf. Table 6).

The abundances derived from our two Ti I lines indicate an α-element behaviour with positive values of [Ti/Fe] for the metal-poor stars, as was traced e.g. for disk stars by Edvardsson et al. (1993), and found for Pop II stars in several studies (see the compilation by Norris et al. 2001, their Fig. 5). For the stars in common with Gratton et al. (2003a) and Jehin et al. (1999) the Ti abundances agree well, while for the 2 stars in common with Nissen & Schuster we obtain higher [Ti/Fe] values by 0.09 and 0.12 dex in [Fe/H], respectively, Fig. 11e and Table 6.

The V abundances obtained by us also suggest systematically positive [V/Fe] values for most Pop II stars, by typically 0.2 dex. Comparisons with other data for common stars cast, however, severe doubts on this result, see Fig. 11f and Table 6.

There is no support from these comparisons that [V/Fe] would be systematically above 0.0. This would also be unexpected, since V is regarded as an iron-peak element and should scale with iron. We also note that Fulbright (2000) found [V/Fe] values close to solar for his large sample of Pop II field stars, most of them dwarfs, as did Johnson (1999) for field giants and Ivans et al. (2001) for globular-cluster giants. As was noted by Ivans et al. (1999) the relatively low ionization energy of V makes [V/Fe] sensitive to the effective temperature adopted for the star; however, as may be seen from Table 5, the higher excitation energy of the line used here reduces the temperature sensitivity so much that an error of 500 K or more is needed to reduce our [V/Fe] values to 0.0. We consider it more probable that our systematically high V abundances may reflect measurement errors due to the weakness of the single V I line, with an equivalent width smaller than 10 mÅ for almost all stars.

Also from Fig. 11g and Table 6 our Cr abundances seem somewhat higher than those derived by others. Again, we may possibly ascribe this result to the difficulty in measuring the single line in our spectra. Anyhow, we have no indication that [Cr/Fe] departs from 0.0 for the Pop II stars, and we can neither verify nor disprove the finding by several authors (e.g., McWilliam et al. 1995; Ryan et al. 1996; Carretta et al. 2002; Fulbright 2002; Cayrel et al. 2004; Barklem et al. 2005) that this abundance ratio becomes subsolar for the most metal-poor stars.

6.7. Nickel

Our Ni abundances are based on a maximum of 7 Ni I lines of different excitation and different strengths. As many previous authors have found, we too find that the abundance ratios [Ni/Fe] stay close to 0.0 at a mean, although there may be a tendency for the scatter in the abundance ratio to increase as [Fe/H] goes below −1. We find a fair agreement with the results of Gratton et al. (2003a), Jehin et al. (1999), and Nissen & Schuster (1997) (Fig. 11h, Table 6). It is noteworthy that the two stars in Fig. 3 departing most from the trends with [Fe/H] = −1.16 and −1.14, respectively, are given similarly low Ni abundances by Jehin et al. (1999). These stars are HD 193901 and HD 194598 with [Ni/Fe] close to −0.20. Gratton et al. (2003a) also find [Ni/Fe] = −0.20 for HD 193901, while they obtain [Ni/Fe] = −0.05 for HD 194598. In view of the generally fair agreement, we conclude that the low [Ni/Fe] values of HD 193901 and HD 194598 seem relatively well established.

6.8. Barium

Our Ba abundances, based on only one blended spectral line with negligible hyperfine-structure and isotopic wavelength shifts (cf. Sect. 3.3.1), show a general behaviour with [Fe/H] in Fig. 3 which is similar to those found by Nissen & Schuster (1997) and McWilliam (1998, his Fig. 2b), while they are a little higher than those of Gratton & Sneden (1988, 1994) and smaller than those of Jehin et al. (1999) and Burris et al. (2000). Thus, we find a rather small scatter for [Fe/H] > −1.5 with
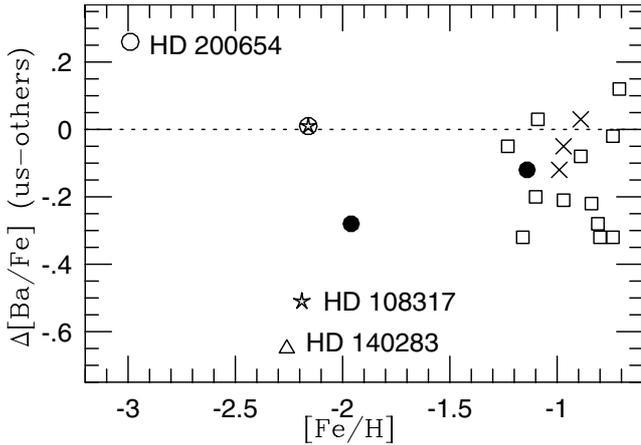
Fig. 12. Comparison of barium abundances with those of Gratton & Sneden (1994) (triangle), Nissen & Schuster (1997) (crosses), McWilliam (1998) (circles), Jehin et al. (1999) (squares), Burris et al. (2000) (stars), and Mashonkina & Gehren (2001) (dots).

[Ba/Fe] solar or slightly sub-solar and a single outlier with high barium abundance, while the mean [Ba/Fe] may decrease, and the scatter increase, for lower metallicities.

When comparing our abundances with those derived by others for common stars we find, however, systematic deviations. These comparisons are summarised in Fig. 12 and Table 6. The basic reason for most of these discrepancies seems to be that the Ba II 6141 Å line is still strong enough in most stars to be severely affected by microturbulence (Table 5) and that e.g. Jehin et al. (1999) have picked systematically lower microturbulence values than our choice of $1.5 \, \text{km s}^{-1}$. In fact, a lowering of our microturbulence parameters by $0.35 \, \text{km s}^{-1}$ would obliterate the mean difference relative to the analyses just mentioned.

Two stars appear Ba rich; the first one is the bright giant HD 196944 with [Ba/Fe] = +1.42. Začs et al. (1998) found the star to be rich in *s* elements and carbon, with [Ba/Fe] = +1.56, while Aoki et al. (2002) derived [Ba/Fe] = +1.10, and a very high lead abundance. Van Eck et al. (2003) also find very high *s*-element abundances for this star. Our second Ba-rich star is HD 17072 with [Ba/Fe] = +0.85. It was spectroscopically investigated by Carney et al. (1998), who in sharp contrast found [Ba/Fe] = −0.39 using three Ba II lines. They derived a 50 K lower effective temperature, 0.6 dex lower log *g*, a $0.6 \, \text{km s}^{-1}$ higher microturbulent velocity, and a 0.2 dex lower iron abundance for the star. Their measured equivalent width for the 6141.7 Å line of 147.6 mÅ is 12 mÅ smaller than our measurement, and using only this line they would have obtained [Ba/Fe] = −0.61, i.e., 1.46 dex below our result. Studying this extreme disagreement, we find that 0.24 dex may be due to the different microturbulent velocities, and 0.05 dex due to the different values of log *g*, 0.02 and 0.03 from differing metallicities and temperatures, and 0.17 dex is due to different log *gf* values while the different equivalent widths only account for 0.16 dex. We cannot trace the remaining difference.
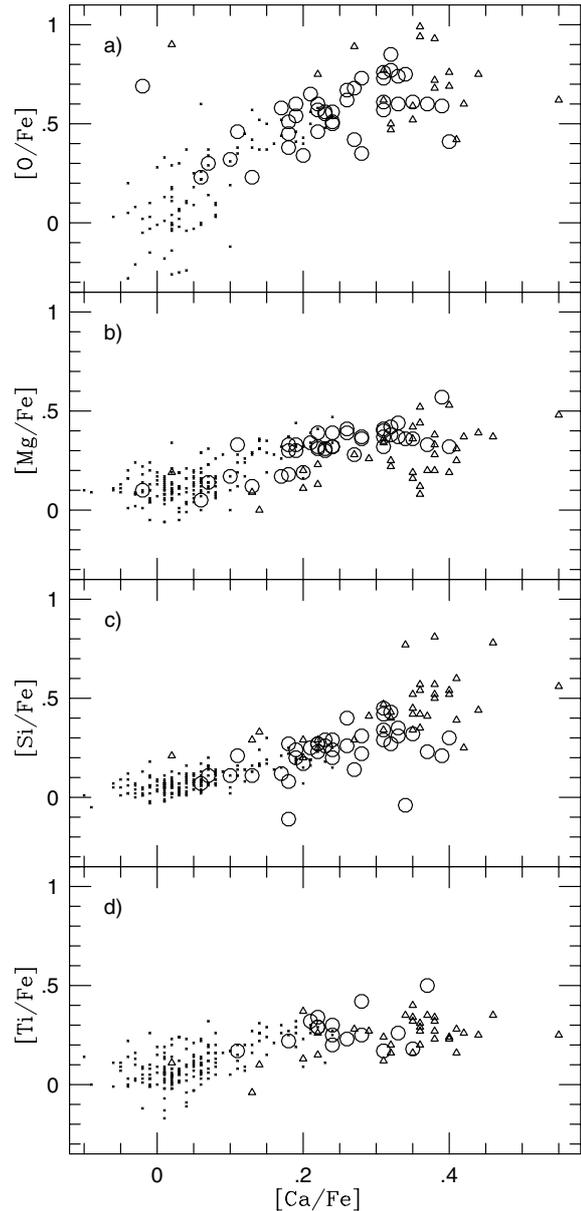
Fig. 13. Relative abundance relations of programme stars (circles, this paper), disk stars (dots, Edvardsson et al. 1993), and extreme Pop II stars from Cayrel et al. (2004) (triangles). (Their [Fe/H] = −4.0 star CS 22949-037 is not seen in panels a and b, since it falls far above the other objects.)

7. Discussion

7.1. Trends in relative abundance

The resulting NLTE abundances of oxygen relative to iron, as derived from the O I IR triplet lines, may systematically increase in [O/Fe] with decreasing metallicity (Fig. 10) for Halo stars. This tendency is, however, not significant. Similar tendencies may also possibly be traced for the α elements Mg (cf. also the discussion of NLTE effects in Sect. 6.5) and Ca in Fig. 3. We have explored whether this co-variation in abundances of the α elements may be observed if the metallicity [Fe/H] is explicitly left out. In Fig. 13 we thus plot the abundances of O, Mg, Si, and Ti relative to Fe directly vs. [Ca/Fe]

for our stars (circles), as well as for the disk stars in Edvardsson et al. (1993) (dots), and find relatively good agreement in slopes between the two samples of stars for the different α elements. We also note that we find similar slopes if we restrict our sample with [Fe/H] < −1.1. We have also extended the overall metallicity range in the figure by adding the 35 extreme Pop II stars of Cayrel et al. (2004) (triangles), of which all but two have metallicities [Fe/H] ranging from −2.5 to −4.4. Their results are by necessity based on a very different set of lines, which are much too strong to be used in our investigation, or by Edvardsson et al. This may cause systematic differences in the results, especially the apparent offsets of the triangles for Mg and Ti relative to Ca in panels b and d.

We studied the correlations for the different data sets by calculating the slopes of least-squares bisector fits (Babu & Feigelson 1992). These give the bisectors of two lines calculated as e.g. [O/Fe] = $a + b$ [Ca/Fe] and [Ca/Fe] = $c + d$[O/Fe]. The slopes b and $1/d$ are often quite different, and the uncertainties in the resulting bisector slopes are relatively large. For [O/Fe] vs. [Ca/H] the slopes are +3.0, +1.5, −1.3, respectively, for the data of Edvardsson et al., for ours, and for those of Cayrel et al. For the combined data the slope is +2.1. It would be interesting to test whether this apparent systematically changing trend with the metallicity of the sample can be confirmed with independent data.

For the three other panels in Fig. 10 the bisector slopes are close to one and show no obvious systematic differences between the different samples. This probably just indicates that the real scatters in Mg, Si, Ca, and Ti vs. Fe have indistinguishable properties within the present limits of measurement accuracy.

Decauwer et al. (2005, Fig. 6) have recently independently demonstrated similar correlations among the different α elements for a smaller sample of Pop II stars.

In trying to interpret the tendencies found we note that the core-collapse supernova model yields, as calculated by Woosley & Weaver (1995), Umeda & Nomoto (2002), and Chieffi & Limongi (2004), show systematically larger amounts of the lighter α elements relative to the heavier ones, as well as to iron, the higher the SN initial mass. That is, an Initial Mass Function varying with metallicity or time in the halo such that the relative number of very massive stars was larger in the population which enriched the early Halo, and with a gradual shift as the evolution progressed, could lead to the correlations observed. Under the assumption that the α elements were made in core-collapse supernovae, we have made simple integrations of the yields of Woosley & Weaver (1995), Umeda & Nomoto (2002), and Chieffi & Limongi (2004) for different values of a single-parameter IMF exponent. These experiments show that in order for variations in the IMF for massive stars to be able to explain the variations in Figs. 13a,b, and c, the exponent has to decrease by two units, e.g., from −1.5 to −3.5 for the halo stars.

For the disk, one could, as in Edvardsson et al. (1993) speculate that significant fractions of Ca and Si were contributed by SNe of type Ia or some other type of object with relatively long lifetimes, in addition to what is provided by the short-lived stars giving rise to core collapse SNe. This

could also be an explanation for the different slopes in our plots. It is possible that the characteristic time scale for SNe Ia to form is relatively short as compared with the formation time of the Halo stars, in particular if a fair fraction of them come from accreted dwarf galaxies with a slow star-formation rate (cf. Nissen & Schuster 1997). An important factor preventing SNe Ia from forming may instead be low metallicity (Kobayashi et al. 1998). Alternative explanations for the slopes in Fig. 13 could be departures from LTE, different for different α elements and varying with [Fe/H]. This possibility should be explored systematically by detailed NLTE calculations.

We also investigated if our data show correlations similar to the interesting relation between the abundances of Y, Ti, and Fe found for Pop II stars by Jehin et al. (1999). Missing data for Y and with limited data for Ti, we looked for relations between Ba, Ca and Fe abundances. A tendency for [Ba/Fe] to increase with [Ca/Fe] for stars around [Fe/H] $\sim$ −1.0 was found, but in view of the uncertainties in the Ba abundances we do not ascribe any clear significance to this tendency.

7.2. Correlations between deviations from mean trends

We computed broken mean relations similar to that in Fig. 10 to define the trends in Fig. 3 and measured deviations from these in the vertical direction. These deviations are denoted by $\delta[X/\text{Fe}]$ for an element X.

An interesting first question is whether the scatter seen in the [Na/Fe] diagram (Fig. 3b) is significant (so-called cosmic scatter), or whether it may be explained as a result of errors in the analysis. The scatter seems to increase for [Fe/H] < −1.0, but the Na lines also get gradually weaker and may be more difficult to measure. We do not find any clear tendency for the deviation $\delta[\text{Na/Fe}]$ to correlate with any other abundance deviation, but possibly with $\delta[\text{Al/Fe}]$, at least in the sense that the stars that seem most under-abundant in Na (for their [Fe/H]) are also under-abundant in Al, Fig. 14. This could contain information on synthesis; Na and Al are both odd nuclei and the result of more complex nucleosynthesis in supernovae than the α elements. We do not find any tendency for $\delta[\text{Na/Fe}]$ to anti-correlate with $\delta[\text{O/Fe}]$, a tendency that might be present if the anomalies found for some globular-cluster stars (e.g., Kraft et al. 1997) were primordial and also represented among field halo stars. We also do not find any clear tendency for $\delta[\text{Na/Fe}]$ to vary systematically with the kinematical characteristics of the stars.

An interesting fact is that different $\delta[X/\text{Fe}]$ correlate for the different elements X = O, Mg, Si, Ca, and Ti; however, the slopes are not identical (Fig. 15). Similar effects show up for halo stars and disk stars, as is seen in Fig. 15 where the stars are denoted differently, depending on whether [Fe/H] is greater or smaller than −1.0. It is important to study whether these correlations do not simply reflect the results of correlated and more or less spurious errors. We first discuss the existence of the correlations as such, and then turn to the origin of the different slopes.
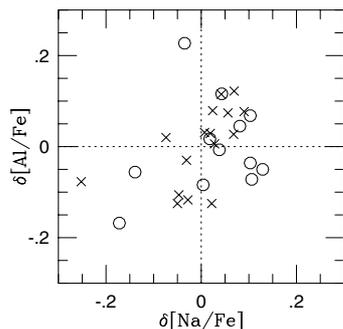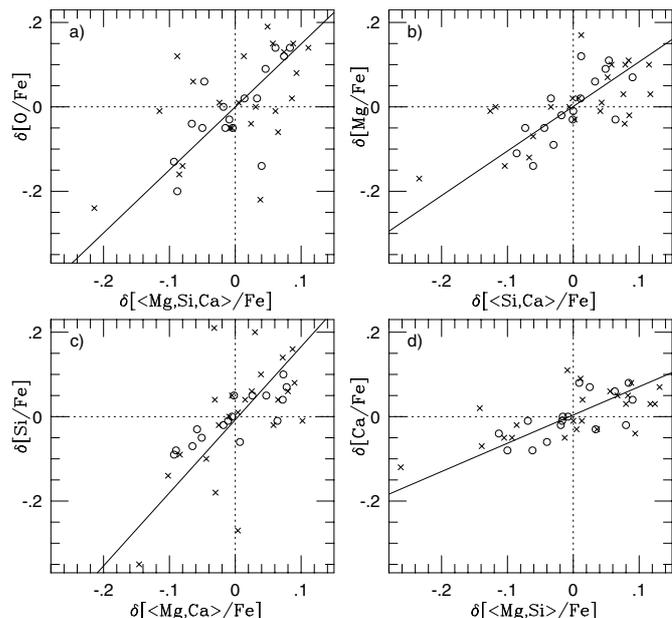
Fig. 14. Scatter correlation plot of Al and Na. $\delta[X/Fe]$ is the deviation in [X/Fe] from a typical [X/Fe] at that [Fe/H]. The circles and crosses represent, respectively, stars with [Fe/H] lower and higher than -1.0.

One way of explaining the correlations would be to advocate that mean errors in [Fe/H] of typically 0.10 would lead to slopes on the order of unity in Fig. 15. However, most explanations for such errors would lead to correlated errors also in e.g. [Mg/H], so that the resulting error in [Mg/Fe] would be reduced. For instance, spurious effective temperature errors of ± 150 K would lead to errors in [Fe/H] of about 0.10 but less than half of that in [Mg/Fe] (Table 6). Thus, with this approach considerably greater errors than 0.10 dex in [Fe/H] seem to be needed to explain the correlations as such. Another more physical explanation for the scatter along lines with unity slope in Fig. 15 would be to claim that there is a true cosmic scatter in [X/Fe] for our Halo stars due to different SNe type Ia contributions of iron. Thus, some stars would come from populations with such a slow star-formation rate that these SNe have already contributed significantly, resulting in comparatively low [α/Fe] values, while other stars (at the same [Fe/H]) come from regions still dominated by core-collapse SNe. Although this explanation is not unrealistic, it would need further confirmation, e.g. from dynamical arguments for a larger sample of stars.

Now we have to ask whether the different slopes for different elements X in Fig. 15 could be the result of correlated errors. Taking the spread along the line with unity slope as given, we wonder whether the different errors in the abundances for the different elements could spread the points from the line such that it leads to differences in slopes. Qualitatively this may be so. The slopes in Fig. 15 for O and Si are about 1.6 (panels a and c), while it is as low as 0.7 for Ca (panel d). The fact that the slope decreases in progression from $X =$ O and Si, Mg, and Ca in Fig. 15 may point in this direction, since we rate the quality of our relative abundances [X/Fe] as increasing in the same order. We have found from numerical experiments that considerable spurious errors are needed, however, on the order of 0.2, 0.2, 0.15, and 0.10, respectively, in [O/Fe], [Si/Fe], [Mg/Fe], and [Ca/Fe] to induce variations in the slopes as great as observed. Although not completely unrealistic, the results from our comparisons with other studies above, as well as analysis of intrinsic errors, suggest only half as great abundance errors. Thus there may be a more physical explanation for the correlations of Fig. 15.

It is natural to explore whether the tendencies of Fig. 15 also show up in the results of other studies. We investigated this for the studies of Gratton et al. (2003a) and

Fig. 15. Correlations among the scatters found in Fig. 3 for different α elements X. $\delta[X/Fe]$ is the deviation in [X/Fe] from a typical [X/Fe] at that [Fe/H]. The circles and crosses represent, respectively, stars with [Fe/H] lower and higher than -1.0. Each line bisects the angle between two linear least-square fits $y = a + bx$ and $x = c + dy$ (Babu & Feigelson 1992).

Nissen & Schuster (1997), which were found (Sect. 6) to be fairly consistent with ours and which contain enough determinations of O, Mg, Si, and Ca abundances. We performed the analyses for these two studies independently, plotting the stars in the [X/Fe] vs. [Fe/H] diagrams with $X =$ Mg, Si, and Ca, fitting lines broken at [Fe/H] $= -1.0$ to the "tendencies", reading off $\delta[X/Fe]$, and plotting the diagrams corresponding to Fig. 15. All stars with data were used, not just those overlapping with our sample; in total, there were 150 stars from Gratton et al. (2003a) and 30 from Nissen & Schuster (1997). The resulting diagrams are displayed in Figs. 16 and 17. It is seen that very similar correlations to ours do result. When the full sample of measurements are used, we find the mean slopes in these diagrams as given in Table 7.

It is noteworthy that the slopes in the [O, Mg, Si, Ca/Fe] vs. [Fe/H] diagrams of Edvardsson et al. (1993) (cf. also Fig. 3 above) for disk stars show a rather similar tendency to the slopes in Figs. 15–17 and in Table 7, with a slope for O being about 1.4 times that of the α elements, while the slope for Ca is about 0.70 of the mean slope. As mentioned above, in Edvardsson et al. this slope difference was tentatively interpreted as the result of variations in the fractions of elements contributed by different types of supernovae. The similarity between the slopes in the panels of Fig. 15 and those in Edvardsson et al. becomes natural if our halo stars were contributed from different environments where star formation has proceeded at different rates with different relative contributions from SNe Ia.

Another possibility would be that we see the result from spurious variations in the IMF at different places in the early Galactic Halo. There is increasing evidence that the IMF varies
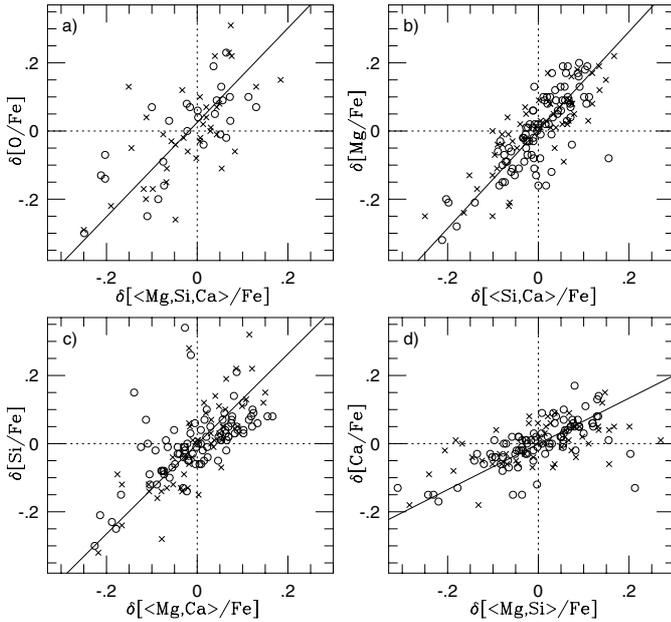
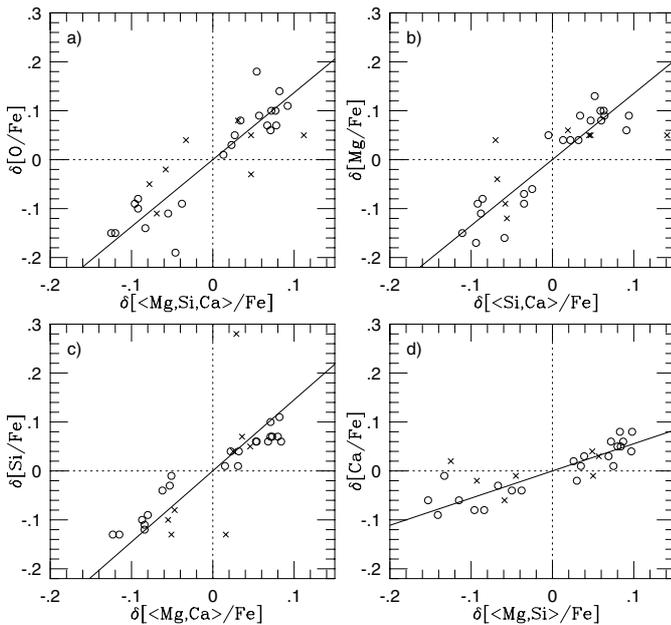**Fig. 16.** Like Fig. 15 but for the data of Gratton et al. (2003a).

Fig. 17. Like Fig. 15 but for the data of Nissen & Schuster (1997).

Table 7. Slopes in correlation diagrams similar to Figs. 15 to 17 for the added sample of measurements by us, Gratton et al. (2003a), and Nissen & Schuster (1997). Data for the subsamples with [Fe/H] > −1.0 and ≤−1.0 are given separately, as well as for the full sample.

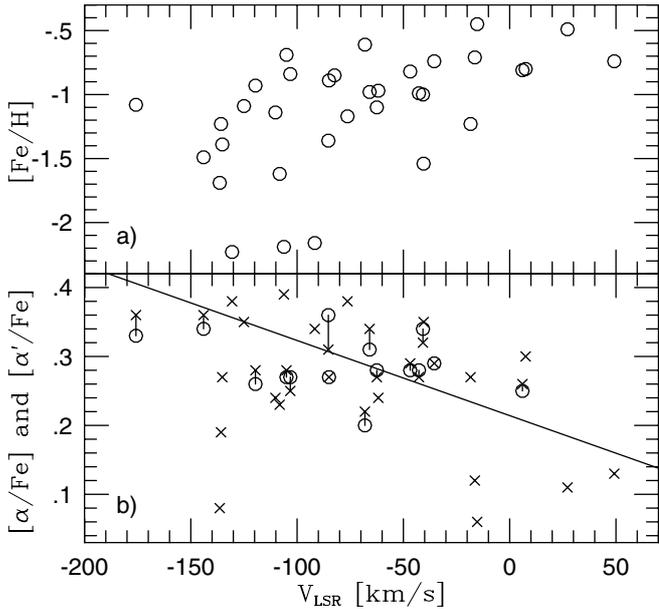| Diagram	[Fe/H]		
	>−1.0	≤−1.0	All
δ[O/Fe] vs. δ[⟨Mg,Si,Ca⟩/Fe]	1.77	1.79	1.84
δ[Mg/Fe] vs. δ[⟨Si,Ca⟩/Fe]	1.26	1.66	1.48
δ[Si/Fe] vs. δ[⟨Mg,Ca⟩/Fe]	1.59	1.04	1.25
δ[Ca/Fe] vs. δ[⟨Mg,Si⟩/Fe]	0.59	0.67	0.64

supernovae, would then be less oxygen-enriched than stars formed in a more massive cloud where very massive stars could also contribute extra oxygen. This scenario might be able to explain the individual star-to-star scatter seen in Fig. 15. It is, however, at odds with the observations for more metal-poor halo stars of Arnone et al. (2004) of very small scatter in relative abundances.

There is also a possibility that the slope differences for different elements, in Fig. 15 and/or those discussed by Edvardsson et al. (see above), merely reflect systematic errors, e.g. varying with metallicity in the latter case. This could then reflect effects of departures from LTE or possibly convection inhomogeneities. The effects shown in Fig. 15 are, however, difficult to explain as being due to errors in effective temperatures or other model parameters as may be found from Table 5. We conclude that another stellar parameter, e.g. related to rotation or magnetic field, may be needed to explain the correlations as results of spurious errors instead of real abundance differences.

7.3. Abundances and kinematics

We divide our metal-poor stars ([Fe/H] < −1.0) into two subsamples, roughly corresponding to the class "accretion component" of Gratton et al. (2003b), here $V_{\rm LSR}$ < −200 km s^{-1} (9 stars), and their "dissipative collapse component", here $V_{\rm LSR}$ > −200 km s^{-1} (17 stars). Gratton et al. suggest that the accretion component stars have a lower mean and a larger spread in [α/Fe] than those of the dissipative collapse component. We find the following differences in mean [X/Fe], $\Delta\langle [X/Fe]\rangle$, and the ratios, $R_{\sigma([X/Fe])}$, of the standard deviation of the scatter between the accretion and dissipative components: $\Delta\langle [Mg/Fe]\rangle$ = −0.03 ± 0.06, $R_{\sigma([Mg/Fe])}$ = 1.7 ± 0.5, $\Delta\langle [Si/Fe]\rangle$ = −0.07 ± 0.08, $R_{\sigma([Si/Fe])}$ = 1.4 ± 0.5, and $\Delta\langle [Ca/Fe]\rangle$ = +0.01 ± 0.07, $R_{\sigma([Ca/Fe])}$ = 3.2 ± 1.1. These R values are statistically significant and consistent with Fig. 6 in Gratton et al. (2003b) but even if our three $\Delta\langle [X/Fe]\rangle$ values are considered together, they are not significantly different from zero. For oxygen, which is presumably formed in the same environments as the α elements, the corresponding figures are $\Delta\langle [O/Fe]\rangle$ = −0.05 ± 0.06, $R_{\sigma([O/Fe])}$ = 1.1 ± 0.35.

Finally, in Fig. 18 we may probably trace the tendencies found by Gratton et al. (2003b) that stars of the dissipative

significantly for star formation occurring in different environments. Thus, a uniform single-parameter IMF, such as the Salpeter IMF, may merely reflect a statistical mean of stars formed in many different regions, while locally the IMF may vary significantly; see, e.g., Elmegreen (2004) and references therein. A type of variable-IMF effect suggested to explain relative-abundance differences similar to ours is that of Jehin et al. (1999) and Decauwer et al. (2005). In the latter paper it is proposed that even with a universal single-parameter IMF, a low-mass star-forming region does not form enough stars to make even a single very massive star, which could later expel very much oxygen. The subsequent generation of stars, born in the same cloud after the first epoch of core-collapse

Fig. 18. Correlations of iron abundances and [α/Fe] with V_{LSR} for stars of the "dissipative collapse component" of Gratton et al. (2003b). In panel b the line shows Eq. (3) of Gratton et al., the circles denote [α/Fe] = $\frac{1}{4}$([Mg/Fe] + [Si/Fe] + [Ca/Fe] + [Ti/Fe]), and the crosses [α'/Fe] = $\frac{1}{3}$([Mg/Fe] + [Si/Fe] + [Ca/Fe]).

component show increasing values of [Fe/H] and decreasing [α/Fe] with increasing rotational velocity V.

8. Conclusions

We have determined chemical abundances for 43 metal-poor solar-type stars, most of them dwarfs or subgiants from the Galactic Halo and old Disk. The abundances were determined for 13 elements, but for 4 elements only one spectral line could be used.

The analysis was strictly differential relative to the Sun, based on 1D LTE model atmospheres both for the Sun and for the stars. Since the Sun is more metal-rich and thus different from all programme stars, systematic errors on the order of 0.15 dex might occur. Another problem may be the effective-temperature scale for which an estimated error of about 100 K may cause systematic errors on the order of 0.07 dex. Other important sources of error, which have not been explored here, are effects of convective inhomogeneities and departures from LTE. The latter were, however, considered in deriving the oxygen abundances from the O I IR triplet lines.

In contrast to what was suggested by Thévenin & Idiart (1999), no overionisation of Fe was found from our single Fe II line, which agrees with the finding of Gratton et al. (2003a). Comparisons with other similar studies show agreement for stars in common, with typical mean differences in abundances significantly less than 0.1 dex. For the elements only represented by one line, the differences may be larger.

We found relations of [X/Fe] vs. [Fe/H], with X = O, Na, Mg, Al, Si, Ca, Ti, and Ni, similar to those that have been found by others. Thus, for X = O we found a slight increase with decreasing [Fe/H], though much smaller than previously found

from the ultraviolet OH bands. Na behaves somewhat differently compared to Al, for which there is an increase, similar to that of Mg, Si, Ca, and Ti. There are some indications that the relative abundance ratios of the α elements vary among the halo stars and that some α abundances relative to Fe may increase with decreasing metallicity. Ni behaves like Fe, as Sc and Cr also seem to do.

We traced a scatter around the mean relations in the [X/Fe] vs. [Fe/H] diagrams that may be partly real. There seem to be correlations between the deviations in [X/Fe] from the mean trends for different α elements X, and the coefficients in these correlations are different. This might be due to larger spurious errors than anticipated and understood, but may also have a more physical explanation. The slope differences are similar to those in the [X/Fe] vs. [Fe/H] diagrams for disk stars, which could result if the halo stars were formed in regions with different (and considerable) characteristic star-formation times. Alternatives would be a widely varying IMF among the halo-star forming clouds or a bias against the formation of very massive stars in a fraction of the clouds. Our results are consistent with those of Gratton et al. (2003b) that stars that do not participate in the rotation of the galactic disk show a lower mean and larger spread in [α/Fe], than stars participating in the general rotation which also show some correlation between [α/Fe] and rotation speed.

We have also identified a number of stars with departing or peculiar abundances, including two Ba stars – one of them known before – and two stars that seem to have low [Ni/Fe] abundances.

The present study is not optimal, a considerably larger sample, with spectra at higher S/N and wider wavelength coverage, can be reached, even for more metal-poor and thus fainter stars. The analysis can be improved by using hydrogen line profiles to set the temperature scale and by using contemporary 3D hydrodynamical models and detailed NLTE modelling. In spite of the existence of fairly consistent results for many stars covered by recent studies, a new even larger homogeneous abundance survey is important. In view of the unsolved problems concerning the origin of the Halo and the early nucleosynthesis, as well as the character of the "Halo-Disk transition" and the unknown origin of the probably physical scatter along the mean abundance trends, such a study is in fact needed. When designing such a study, one should place emphasis on the selection criteria applied. Until now, in all the studies of general Halo stars known to us the kinematic criteria have been introduced in a more or less ad-hoc way.

improvements.

References

Aller, L. H., & Greenstein, J. L. 1960, ApJS, 5, 139

Alonso, A., Arribas, S., & Martínez-Roger, C. 1995, A&A, 297, 197

Alonso, A., Arribas, S., & Martínez-Roger, C. 1996, A&A, 313, 873

Aoki, W., Ryan, S. G., Norris, J. E., et al. 2002, ApJ, 580, 1149

Arnett, W. D. 1971, ApJ, 166, 153

Arnone, E., Ryan, S. G., Argast, D., Norris, J. E., & Beers, T. C. 2005, A&A, 430, 507

Arpigny, C., & Magain, P. 1983, A&A, 127, L7

Asplund, M., & García Pérez, A. E. 2001, A&A, 372, 601

Asplund, M., Grevesse, N., Sauval, A. J., Allende Prieto, C., & Kiselman, D. 2004, A&A, 417, 751

Asplund, M., Gustafsson, B., Kiselman, D., & Eriksson, K. 1997, A&A, 318, 521

Asplund, M., Gustafsson, B., Kiselman, D., & Eriksson, K. 1997, A&A, 323, 286

Asplund, M., Nordlund, Å., Trampedach, R., & Stein, R. F. 1999, A&A, 346, L17

Babu, G. J., & Feigelson, E. D. 1992, Commun. Stat. Part B, 21(2), 533

Barbuy, B. 1988, A&A, 191, 121

Bard, A., Kock, A., & Kock, M. 1991, A&A, 248, 315

Barklem, P. S., Piskunov, N., & O'Mara, B. J. 2000, A&AS, 142, 467

Barklem, P. S., Christlieb, N., Beers, T. C., et al. 2005, A&A, in press [arXiv:astro-ph/0505050]

Bashkin, S., & Stoner, J. O. Jr. 1975, Atomic Energy Levels and Grotrian Diagrams, 1–4 (Amsterdam: North-Holland Publishing Company)

Baumüller, D., & Gehren, T. 1997, A&A, 325, 1088

Baumüller, D., Butler, K., & Gehren, T. 1998, A&A, 338, 637

Bensby, T., Feltzing, S., & Lundström, I. 2003, A&A, 410, 527

Blackwell, D. E., Lynas-Gray, A., & Smith, G. 1995, A&A, 296, 217

Boesgaard, A. M., King, J. R., Deliyannis, C. P., & Vogt, S. S. 1999, AJ, 117, 492

Boesgaard, A. M., King, J. R., Deliyannis, C. P., & Vogt, S. S. 1999, AJ, 118, 2542

Burris, D. L., Pilachowski, C. A., Armandroff, T. E., et al. 2000, ApJ, 544, 302

Carney, B. W. 1983, AJ, 88, 623

Carney, B. W., Lee, J.-W., & Habgood, M. J. 1998, AJ, 116, 424

Carretta, E., Gratton, R., Cohen, J. G., et al. 2002, AJ, 124, 481

Cayrel, R., Depagne, E., Spite, M., et al. 2004, A&A, 416, 1117

Cayrel de Strobel, G., Soubiran, C., Friel, E. D., et al. 1997, A&AS, 124, 299

Chieffi, A., & Limongi, M. 2004, ApJ, 608, 405

Decauwer, H., Jehin, E., Parmentier, G., & Magain, P. 2005, A&A, in press

Dehnen, W., & Binney, J. J. 1998, MNRAS, 298, 387

Edvardsson, B., Andersen, J., Gustafsson, B., et al. 1993, A&A, 275, 101

Elmegreen, B. G. 2004, MNRAS, 354, 367

Eggen, O. J., Lynden-Bell, D., & Sandage, A. R. 1962, ApJ, 136, 748

Egret, D. 1986, Bull. Inform. CDS No. 30

ESA 1997, The Hipparcos and Tycho Catalogues, ESA SP–1200

Fuhrmann, K. 1998, A&A, 338, 161

Fulbright, J. P. 2000, AJ, 120, 1841

Fulbright, J. P. 2002, AJ, 123, 404

García Pérez, A. E., Asplund, M., Nissen, P. E., Primas, F., & Gustafsson, B. 2005, A&A, submitted

Gehren, T., Butler, K., Mashonkina, L., et al. 2001, A&A, 366, 981

Gehren, T., Liang, Y. C., Shi, J. R., et al. 2004, A&A, 413, 1054

Gosset, E., & Magain, P. 1993, ESO Messenger, 73, 13

Gratton, R. G., Carretta, E., Matteucci, F., & Sneden, C. 1996, in Formation of the Galactic Halo....Inside and Out., ed. H. Morrison, & A. Sarajedini, ASP Conf. Ser., 92, 307

Gratton, R. G., Carretta, E., Matteucci, F., & Sneden, C. 2000, A&A, 358, 671

Gratton, R. G., Carretta, E., Claudi, R., et al. 2003a, A&A, 404, 187

Gratton, R. G., Carretta, E., Desidera, S., et al. 2003b, A&A, 406, 131

Gratton, R. G., & Sneden, C. 1988, A&A, 204, 193

Gratton, R. G., & Sneden, C. 1994, A&A, 287, 927

Grevesse N., & Sauval, A. J. 1998, Space Sci. Rev., 85, 161, Cambridge Philosophical Society

Grønbech, B., & Olsen, E. H. 1976, A&AS, 25, 213

Grønbech, B., & Olsen, E. H. 1977, A&AS, 27, 443

Hakkila, J., Meyers, J. M., Stidham, B. J., & Hartmann, D. H. 1997, AJ, 114, 2043

Hauck, B., & Mermilliod, M. 1998, A&AS, 129, 431

Holweger, H. 1971, A&A, 10, 128

Holweger, H. 1973, A&A, 26, 275

Holweger, H., Heise, C., & Kock, M. 1990, A&A, 232, 510

Holweger, H., & Müller E. A. 1974, Sol. Phys., 39, 19

Israelian, G., García López, R. J., & Rebolo, R. 1998, ApJ, 507, 805

Ivans, I. I., Sneden, C., Kraft, R. P., et al. 1999, AJ, 118, 1273

Ivans, I. I., Kraft, R. P., Sneden, C., et al. 2001, AJ, 122, 1438

Jehin, E., Magain, P., Neuforge, C., et al. 1999, A&A, 341, 241

Johnson, D. R. H., & Soderblom, D. R. 1987, AJ, 93, 864

Johnson, J. 1999, Ph.D. Thesis, Univ. California, Santa Cruz

Karlsson, T., & Gustafsson, B. 2001, A&A, 379, 461, A&A, 386, 884

King, J. R. 1993, AJ, 106,1206

Kiselman, D. 1991, A&A, 245, L9

Kiselman, D. 1993, A&A, 275, 269

Kraft, R. P., Sneden, C., Smith, G. H., et al. 1997, AJ, 113, 279

Kobayashi, C., Tsujimoto, T., Nomoto, K., Hachisu, I., & Kato, M. 1998, ApJ, 503, L55

Kupka, F., Piskunov, N. E., Ryabchikova, T. A., et al. 1999, A&AS, 138, 119

Kurucz, R. L. 1989, Atomic line data for Ca through Ni, private communication

Kurucz, R. L., Furenlid, I., Brault, J., & Testerman, L. 1984, Solar flux atlas from 296 to 1300 nm National Solar Observatory Atlas, Sunspot, New Mexico: National Solar Observatory

Lindgren H. (unpublished)

Mäckle, R., Holweger, H., Griffin, R., & Griffin, R. 1975, A&A, 38, 239

Magain, P. 1984, A&A, 134, 189

Magain, P. 1987, A&A, 179, 176

Magain, P. 1989, A&A, 209, 211

Magain, P., & Zhao, G. 1996, A&A, 305, 245

Mashonkina, L., & Gehren, T. 2001, A&A, 376, 232

McWilliam, A. 1997, ARA&A, 35, 503

McWilliam, A. 1998, AJ, 115, 1640

McWilliam, A., Preston, G. W., Sneden, C., & Shectman, S. 1995, AJ, 109, 2757

Nissen, P. E., Primas, F., Asplund, M., & Lambert, D. L. 2002, A&A, 390, 235

Nissen, P. E., Høg, E., & Schuster, W. J. 1997, ESA SP-402, 225

Nissen, P. E., Gustafsson, B., Edvardsson, B., & Gilmore, G. 1994, A&A, 285, 440

Nissen, P. E., Primas, F., Asplund, M., & Lambert, D. L. 2002, A&A, 390, 235

Nissen, P. E., & Schuster, W. J. 1997, A&A, 326, 751

Nordström, B., Mayor, M., Andersen, J., et al. 2004, A&A, 418, 989

Norris, J. E., Ryan, S. G., & Beers, T. C. 2001, ApJ, 561, 1034

Olsen, E. H. 1983, A&AS, 54, 55

Olsen, E. H. 1988, A&A, 189, 173

Olsen, E. H. 1993, A&AS, 102, 89

Reddy, B. E., Tomkin, J., Lambert, D. L., & Allende Prieto, C. 2003, MNRAS, 340, 304

Ryan, S. G., Norris, J. E., & Beers, T. C. 1996, ApJ, 471, 254

Saxner, M., & Hammarbäck, G. 1985, A&A, 151, 372

Searle, L., & Zinn, R. 1978, ApJ, 225, 357

Schuster, W. J., & Nissen, P. E. 1988, A&AS, 73, 225

Schuster, W. J., & Nissen, P. E. 1989, A&A, 221, 65

Shetrone, M. D. 1996, AJ, 112, 2639

Spite, M., & Spite, F. 1980, A&A, 89, 118

Thévenin, F., & Idiart, T. 1999, ApJ, 521, 753

Timmes, F. X., Woosley, S. E., & Weaver, T. A. 1995, ApJS, 98, 617

Umeda, H., & Nomoto, K. 2002, ApJ, 565, 385

Unsöld, A. 1955, Physik der Sternatmosphären, 2nd ed. (Berlin: Springer Verlag)

VandenBerg, D. A., & Bell, R. A. 1985, ApJS, 58, 561

VandenBerg, D. A., Swenson, F. J., Rogers, F. J., et al. 2000, ApJ, 532, 430

Van Eck, S., Goriely, S., Jorissen, A., & Plez, B. 2003, A&A, 404, 291

Woosley, S. E., & Weaver, T. A. 1995, ApJS, 101, 181

Wiese, W. L., & Martin, G. A. 1980, NSRDS-NBS 68, Wavelengths and Transition Probabilities for Atoms and Atomic Ions, Part 2. US Government Printing Office, Washington, DC

Začs, L., Nissen, P. E., & Schuster, W. J. 1998, A&A, 337, 216

Zhao, G., & Magain, P. 1991, A&A, 244, 425